AD_____

Award Number: W81XWH-06-1-0618

TITLE: Gold Nanoparticle Contrast Agents in Mammography: A Feasibility Study

PRINCIPAL INVESTIGATOR: Andrew D. A. Maidment, Ph.D.

CONTRACTING ORGANIZATION: University of Pennsylvania
Philadelphia, PA 19104

REPORT DATE: August 2008

TYPE OF REPORT: Final

PREPARED FOR: U.S. Army Medical Research and Materiel Command
Fort Detrick, Maryland 21702-5012

REPORT DOCUMENTATION PAGE

Form Approved
OMB No. 0704-0188

1. REPORT DATE	2. REPORT TYPE	3. DATES COVERED
1 Aug 2008	Final	15 Jul 2006 – 14 Aug 2008

4. TITLE AND SUBTITLE

Gold Nanoparticle Contrast Agents in Mammography: A Feasibility Study

5a. CONTRACT NUMBER

5b. GRANT NUMBER
W81XWH-06-1-0618

5c. PROGRAM ELEMENT NUMBER

6. AUTHOR(S)

Andrew D. A. Maidment, Ph.D.

E-Mail: Andrew.Maidment@uphs.upenn.edu

5d. PROJECT NUMBER

5e. TASK NUMBER

5f. WORK UNIT NUMBER

7. PERFORMING ORGANIZATION NAME(S) AND ADDRESS(ES)

University of Pennsylvania
Philadelphia, PA 19104

8. PERFORMING ORGANIZATION REPORT NUMBER

9. SPONSORING / MONITORING AGENCY NAME(S) AND ADDRESS(ES)
U.S. Army Medical Research and Materiel Command
Fort Detrick, Maryland 21702-5012

10. SPONSOR/MONITOR'S ACRONYM(S)

11. SPONSOR/MONITOR'S REPORT NUMBER(S)

12. DISTRIBUTION / AVAILABILITY STATEMENT
Approved for Public Release; Distribution Unlimited

13. SUPPLEMENTARY NOTES

14. ABSTRACT

The successful translation of molecular imaging to mammography and digital breast tomosynthesis would allow clinical molecular imaging of the breast. This is a potentially more sensitive approach to early breast cancer detection, especially in women at high risk. Bioconjugated gold (Au) nanoparticle (NP) imaging agents, used in conjunction with digital mammography and breast tomosynthesis, should provide improved lesion conspicuity. Au-NP are exceptionally attenuating at mammographic energies; even very low concentrations are theoretically detectable. The primary aim of this study was to prove that Au-NP can act as a viable mammographic contrast agent. We successfully synthesized bioconjugated HER2/neu Au-NP. Using a multifunctionalization method with PEG and an anti-Her2 neu affibody, we were able to create nanoparticles which were stable in serum. These data are sufficient to begin in vitro studies to determine whether mammography molecular imaging agents are feasible.

15. SUBJECT TERMS
Breast Cancer, X-ray contrast agent, Gold Nanoparticles, Her2/neu

16. SECURITY CLASSIFICATION OF:			17. LIMITATION OF ABSTRACT	18. NUMBER OF PAGES	19a. NAME OF RESPONSIBLE PERSON
a. REPORT	b. ABSTRACT	c. THIS PAGE			19b. TELEPHONE NUMBER *(include area code)*
U	U	U	UU	71	USAMRMC

Table of Contents

1. Introduction

Bioconjugated gold (Au) nanoparticle (NP) imaging agents, used in conjunction with digital mammography and breast tomosynthesis, should result in significantly improved lesion conspicuity. Molecular imaging agents targeted to bind to specific ligands have been proposed for many imaging modalities[1]. However, we are unaware of any molecular imaging agents proposed for mammography; the most common breast imaging method.

We proposed to study the feasibility of mammographic molecular imaging through *in vitro* "mock tumor" studies of analogues of Herceptin (a monoclonal antibody that binds to HER2/neu) conjugated to Au-NP. Au-NP are exceptionally attenuating at mammographic energies; thus, even very low concentrations are theoretically detectable. We calculate that to achieve a 5% change in attenuation at 17.5 keV (Mo K_α) we would require ten 100μm dia. NP per cell; this would allow the detection of a 5 mm dia. tumor at a clinical mammographic dose (1.8 mGy). Using similar agents for thermoacoustic tomography, Copland[2] achieved significant tissue enhancement with a binding density of 18 NP per cell. The combination of such contrast agents with dual-energy subtraction breast tomosynthesis would allow high-resolution cross-sectional molecular imaging *in vivo* and trivial fusion of functional and anatomic images.

In this grant, we proposed to demonstrate in proof-of-principle the viability of Au-NP targeted mammographic molecular imaging agents. We investigated fabrication feasibility and contrast sensitivity of these agents. These data will be used for submission of a grant to develop such imaging agents further.

2. Body

2.1. Research Overview

The research conducted over the past two years has been directed towards synthesizing molecular imaging agents for use with emerging breast imaging modalities such as digital breast tomosynthesis (DBT) and breast computed tomography (BCT). Molecular imaging agents use specific biomarkers to target tissues or organs so that they can be easily distinguished from their immediate environment.

We have opted to use gold in the form of spherical nanoparticles as the building block for the imaging agents because of the high x ray attenuation of gold at low mammographic energies. The nanoparticles were conjugated with an affibody targeting the epidermal growth factor receptor protein, HER2/neu. Studies have shown that HER2/neu is over-expressed in 25-30 % of all breast cancers. Breast cancer cell lines are being cultured to investigate the binding and uptake of these nanoparticles, and to measure the x-ray imaging properties. These data will provide the data necessary to determine the potential effectiveness of the conjugated gold nanoparticles as contrast agents.

The research therefore consists of three major subsections:

(i) Synthesis and functionalization of gold nanoparticles

(ii) Growth and culturing of breast cancer cell lines

(iii) Mock tumor studies.

We were able to successfully complete 2 of the 3 major aims and the results obtained are presented herewith. Difficulties arose when the originally proposed nanoparticles were placed in media and coalesced. This required the development of the multifunctionalization approach described in Section 2.2.6. As a result, it was not possible to complete the mock tumor studies. In hindsight, these studies were probably ill-conceived. Future research is planned with *in vitro* incubation of the nanoparticles with appropriate cell lines followed by TEM imaging, and *in vivo* studies in nude mice.

2.2. Results

2.2.1. Synthesis of gold nanoparticles

Gold nanoparticles (AuNP) have been synthesized using a modified Turkevich method[3]. This involves the reduction of a gold precursor in the presence of a surface stabilizing agent. We have used gold (III) chloride as the gold metal precursor and sodium citrate as the reducing agent. The latter serves a dual function as both the reducing agent as well as the surface stabilizing molecule. When certain environmental conditions are met in the synthesis of the AuNP, citrate anions will coat the surface of the AuNP, thus preventing them from aggregating out of the solution. The final size and shape distribution is heavily dependant on the molar ratio between the gold(III) chloride and the sodium citrate. We have used molar ratios of 4:1, 3:1, 2:1 and 1:1 to obtain successively larger sized nanoparticles.

Initially, we used the procedure set forth by Grabar *et al.*[4], to synthesize citrate-capped AuNP with an expected diameter in the range of 13nm using a molar ratio of 4:1 between the gold and the sodium citrate. Briefly, 0.20g of gold (III) chloride trihydrate ($HAuCl_4.3H_2O$) was dissolved with 500ml of triple-distilled water in a 1L round-bottom flask to which a Teflon-coated magnetic stir bar was added. The flask was then placed atop a heating mantle and magnetic stirrer and the gold solution was brought to a boil. A quantity (0.57g) of sodium citrate dihydrate ($C_6H_5Na_3O_7.2H_2O$) was then dissolved in 50ml of deionized water and then added to the boiling gold solution. Upon addition of the sodium citrate, the solution rapidly changed color from a pale yellow to a dark burgundy. Heating was continued for an additional 10 minutes after which the hearing mantle was removed and the solution was stirred for an extra 15 minutes. The resulting colloidal solution was allowed to cool overnight after which it was filtered through a 0.2 μm membrane filter.

The AuNPs produced using a 4:1 ratio remained a light burgundy, whereas those synthesized with a 3:1 ratio were more purple-red. Finally, the particles produced using the lowest citrate to gold ratio of 1:1, were dark brown-purple.

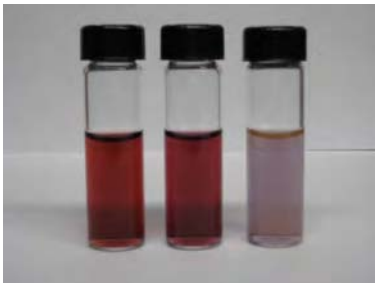

Figure 1. Gold Nanoparticle solutions of various diameters. From left to right, using molar ratios of 4:1 (light burgandy), 3:1 (purple-red), 1:1 (dark brown-purple)

2.2.2. AuNP diameter measurements

Small angle x ray scattering (SAXS) was used to determine the size and distribution of the AuNP[5]. A small sample of the AuNP was placed in a cuvette, sealed with epoxy, and then placed in the path of an x ray beam of known energy. The intensity of the scattered beam is measured at various scattering angles, and a Guinier plot[5] (logarithm of intensity vs. scattering vector) was obtained. The plot is modeled as a series of functions, such as polynomial and Rayleigh functions, to determine best the radius of the AuNP in solution. A subset of these results is shown in Table 1.

Using a molar ratio of 4:1 between the gold (III) precursor and sodium citrate, we obtained AuNP with a diameter of approximately 14nm

Table 1. Radius of AuNP determined from SAXS

Rayl Radius	Value	Standard Error	Lower Limit	Upper Limit
(in nm)	6.9810	0.0066	6.9512	7.0117

The AuNPs produced using a molar ratio of 3:1 between the gold salt and sodium citrate were found to be in the range of 21 nm, while those produced using the 1:1 ratio were in excess of 100 nm.

2.2.3. UV-Vis spectrum of AuNPs

Using the extinction coefficients for gold nanoparticles provided in the literature[6], and the absorption spectrum of the AuNP solution in the UV-Vis range (Figure 1), we were able to determine the concentration of the AuNP in solution to be 9nM. The UV-Vis spectra of the AuNP shows a peak in the absorbance at a wavelength of 518 nm. This peak is typical of AuNP in solution due to the excitation of surface plasmons on the gold nanostructure[6].

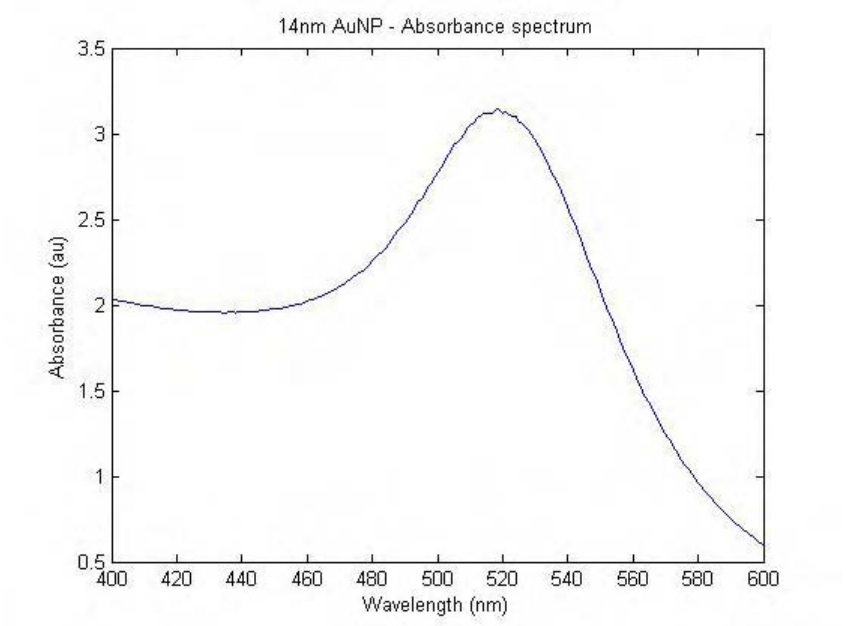

Figure 2. Uv-Vis absorbance spectra of the 14nm AuNP in solution

2.2.4. Images of citrate-capped AUNP

Transmission electron microscopy (TEM) was used to obtain images of the 21 nm citrate-capped nanoparticles in solution A drop of the AuNP solution was placed on a carbon grid and allowed to dry for 6 hours prior to imaging. The grid was then imaged using a high-resolution transmission electron microscopy, and the images obtained are shown in Figure 3. The particles were all spherical in shape and many of them were found to have clumped together. This is thought to be because of the weak stabilizing force of the citrate anions on the AuNP surface. The repulsive force between the negatively charged AuNPs is insufficient to prevent clumping of the particles.

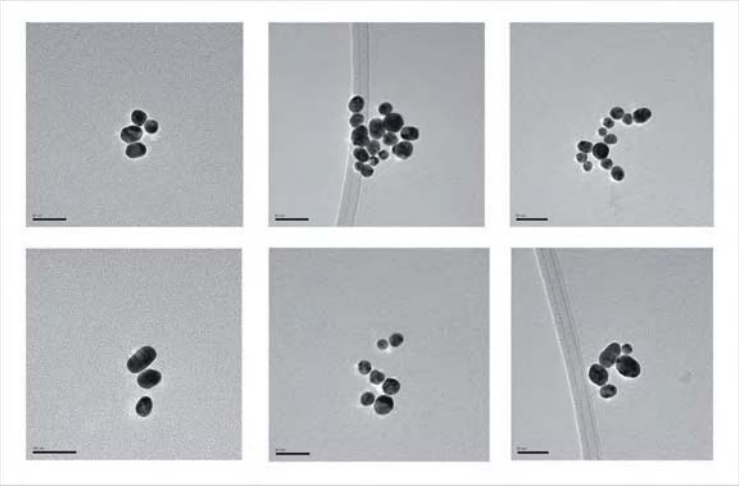

Figure 3. TEM images of 21nm AuNPs.

2.2.5. Stabilization of AuNP with PEG

The citrate-capped AuNP were shown to be unstable in high ionic strength biological media. When 200µl of 14nm AuNP is added to 400µl of phosphate buffered saline (PBS) solution, a buffer used to mimic the extra cellular conditions of the human body, the AuNP were observed to aggregate out of the solution. The UV-Vis spectrum of the aggregated AuNP solution showed a large red-shift and spreading of the absorbance peak as the color of the solution changed from a burgundy-red to a purple blue.

In order to improve their stability, the AuNP will first be conjugated to polyethylene glycol (PEG) peptides in order to increase their stability in salt solutions, as well as enhance their stealth properties *in vivo*. The PEG molecules obtained for the conjugation had an average molecular weight of 5000 Daltons, and were capped with an unreactive methyl group on one end and a thiol (-SH) group on the other.

3ml of 21 nm AuNP (2.81 nM) was mixed with 212µl of 0.5µg/µl PEG-thiol solution in a 10ml round-bottom flask, and stirred at room temperature for 1 hour. The solution was then centrifuged at 11,400g for 20 minutes, and the AuNP pellet was redissolved in 2ml of deionized water after the supernatant had been removed. The resulting AuNP-PEG solution was stored at room temperature. The UV-Vis spectrum (Figure 2) of the AuNP-PEG showed a red shift of 3nm in the absorbance peaks between the conjugated and unconjugated AuNP. The shift in the spectrum indicates that the PEG molecules have successfully replaced the citrate anions and bound to the AuNP surface[6].

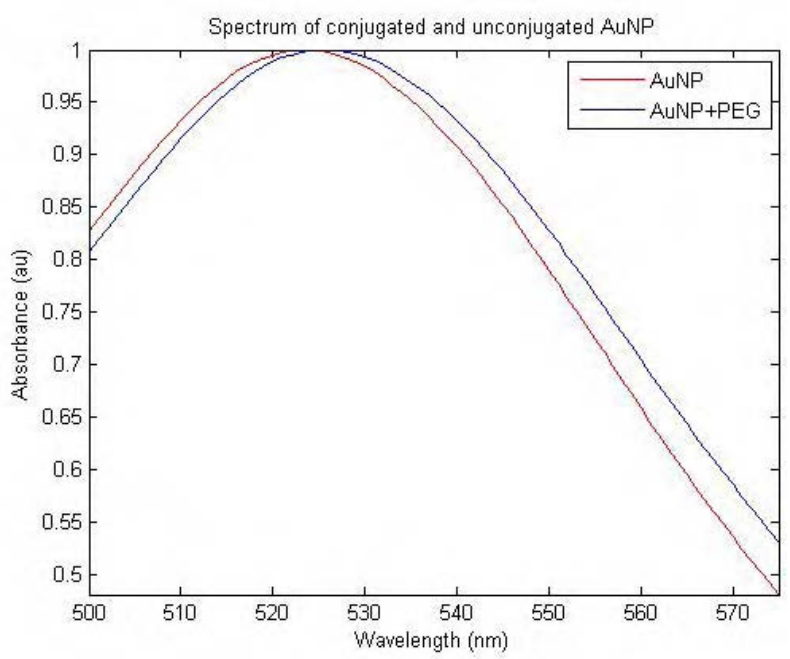

Figure 4. Spectrum of conjugated and unconjugated AuNP

The stability of the conjugated AuNP was testing by adding 200µl of AuNP-PEG solution to 400µl of PBS solution. There have been no observable changes in the color of the solution and the spectrum of the AuNP-PEG was unchanged.

2.2.6. Functionalization of AuNP with PEG and affibodies.

The AuNP have been functionalized with admixtures of PEG and the anti-HER2/neu affibody on the surface of the AuNP. Two forms of the anti-HER2/neu affibody were obtained: an unconjugated affibody in which the C-terminus has been linked to cysteine and a fluorescein-conjugated molecule, in which the C-terminal cysteine has been conjugated to a maleimide-activated fluorescein agent. These affibodies have the same binding sites and binding properties as the native antibodies with the added advantage that they are several times smaller than regular antibodies. The smaller size means that they should exhibit tumor-to-blood ratios that exceed typical values for monoclonal antibodies. The unconjugated molecule will be used for the multi-functionalization of the AuNP whereas the fluorescein-conjugated affibodies will be used in flow cytometry and immuno-staining to compare the expression of the HER2/neu surface protein between the cell lines obtained.

Multi-functionalization of the AuNP with a mixed monolayer of PEG and anti-HER2/neu affibody was carried out sequentially, in two discrete steps as documented by Liu *et al*[7]. First, 3ml of the 21nm AuNP solution was mixed with 170µL of 0.5µg/µL of PEG-thiol solution in a 10ml round-bottom flask, and stirred at room temperature for 1 hour. The solution was then centrifuged at 11,400g for 20 minutes, and the resulting pellet was resuspended in 250µL of 1% PBS solution. 85µg of 1mg/mL anti-HER2/neu affibody was then added to the PEGylated AuNP solution. The mixture was stirred for 1 hour at

room temperature, and then centrifuged at 11,400g for 26 minutes. The AuNP-PEG-affibody pellet was then redissolved in 500μL of PBS.

The introduction of a mixed monolayer of PEG chains and anti-HER2/neu affibodies onto the AuNP surface, resulted in a 2nm red shift in the absorbance peaks compared to the PEGylated AuNPs (Figure 5). Table 2 shows the gradual shift in the absorbance band of the AuNP solution, as different components are added to the surface.

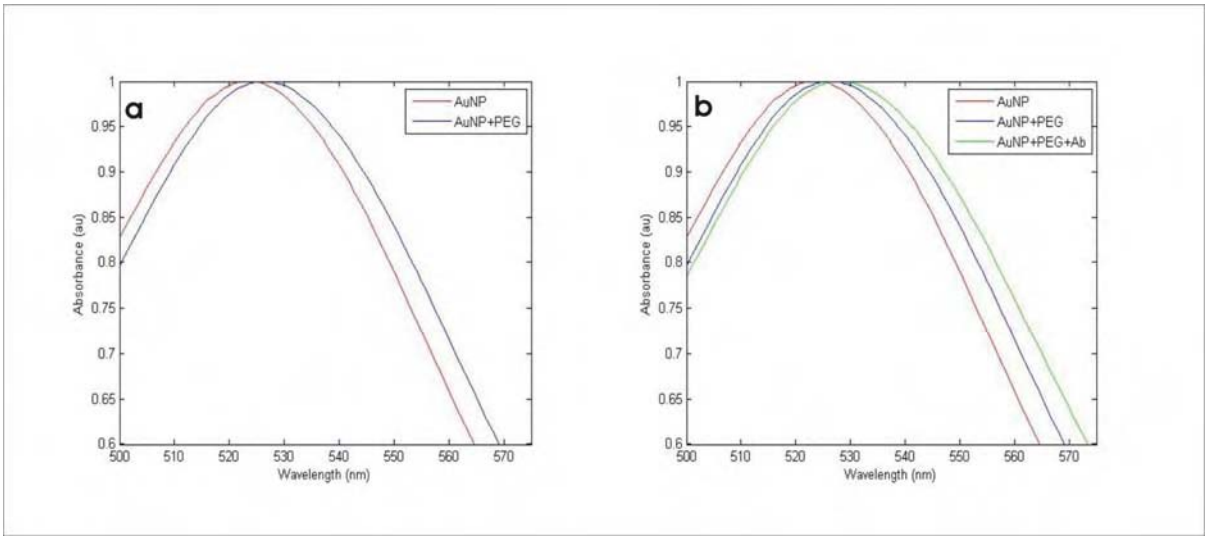

Figure 5. Result of conjugating PEG chains (a) , PEG chains and anti-HER2/neu affibodies (b) onto the surface of 21 nm AuNPs

Table 2. Red shift of 21 nm AuNPs

	Peak wavelength of SPR band (nm)
AuNP (unconjugated, citrate-capped)	523
AuNP + PEG	526
AuNP + PEG + anti-HER2/neu affibody	528

2.2.7. Growth and culturing of breast cancer cell lines

Two breast cancer cell lines, BT-474 and MDA-MB-231 have been obtained. These particular cell lines have been chosen for their differences in the levels of expression of HER2/neu on their cell surface. BT-474 exhibits amplified expression of the protein whereas MDA-MB-231 has a low-to-normal protein expression. Both cell lines have been extensively studied and have been shown to form tumors in nude mice[8,9].

BT-474 cells are grown in RPMI-1640 medium while the MDA-MB-231 cells (Figure 3) are grown in Dulbecco's Modified Eagle's Medium (DMEM). All media must be supplemented with 10% fetal bovine serum (FBS), 1% L-glutamine and 1% penicillin/ streptavidin. Both cell lines are be cultivated in T-75 flasks and incubated at room temperature (37 ˚C) and 5% CO_2. The media must be renewed 2 to 3 times a week, and a subcultivation ratio of 1:2 is being used for both cell lines.

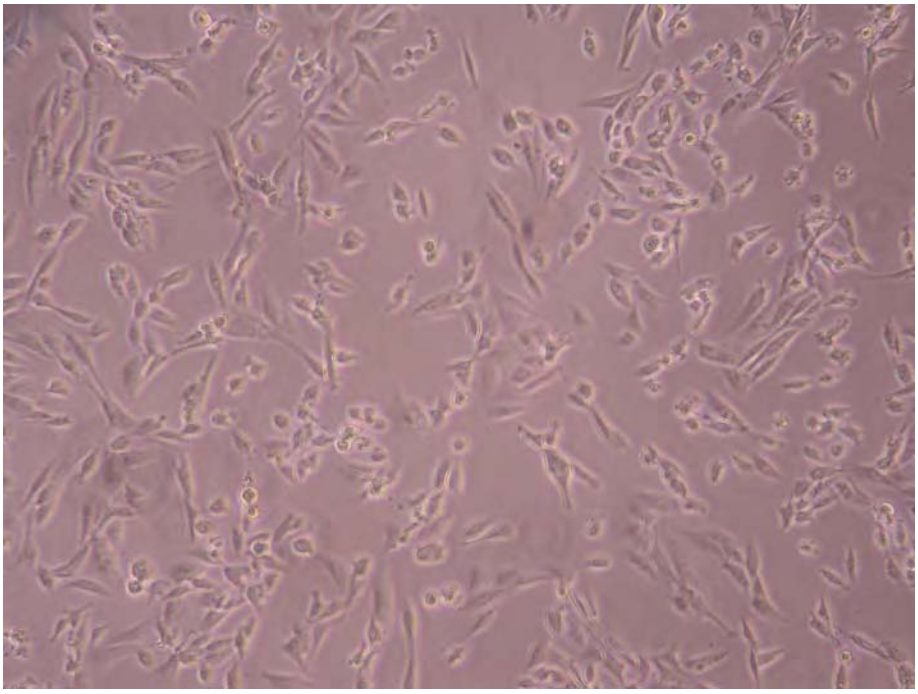

Figure 6. MDA-MB-231 cells

The cell lines will serve two primary purposes (beyond the scope of the current grant). The first is to study the binding and internalization patterns of the affibody-receptor complex in *vitro*. The second is to form tumors in nude mice to determine the effectiveness and uptake rates of the AuNP *in vivo*.

3. Key Research Accomplishments:

We have successfully synthesized spherical gold nanoparticles with controlled diameters of between 13 and 100 nm. We have successfully conjugated both PEG (an inert control) and admixtures of PEG and anti-HER2/neu affibodies to the gold nanoparticles. We have demonstrated that the conjugated nanoparticles are stable in serum. We have established two working cell lines. We are currently engaged in experiments to measure affinity of the various conjugates to tumor cells which over- and under-express the HER2/neu antigen. X-ray imaging tests will follow.

4. Reportable Outcomes:

1) R Karunamuni, AV Popov, H Qiao, S-J Park, ADA Maidment. HER2/neu-targeted Gold Nanoparticles Contrast Agents for Mammography and Tomosynthesis. *DOD Era of Hope*, Baltimore MD, June 2008.
2) The CDMRP FY08 Predoctoral Traineeship grant "HER2-Targeted Gold Nanoparticle Contrast Agent for Digital Breast Tomosynthesis and Computed Tomography" (BC083334 – R Karunamuni, PI).
3) Master's Thesis: "HER2/neu-targeted Gold Nanoparticle contrast agents for Digital Mammography and Digital Breast Tomosynthesis" by Roshan Karunamuni in Bioengineering, University of Pennsylvania, August 2008.

5. Conclusions:

We have successfully been able to produce bioconjugated gold nanoparticles. Molecular imaging is widely seen as the future of medical imaging. However, methods developed to date are only suitable *in vitro* or in laboratory animals. The successful translation of molecular imaging to mammography and digital breast tomosynthesis would allow clinical molecular imaging of the breast. This is a potentially more sensitive approach to early breast cancer detection, especially in women at high risk.

6. References:

1. Rotello V. Nanoparticles: Building Blocks for Nanotechnology. New York: Kluwer Academic Press; 2004.
2. Copland JA, Eghtedari M, Popov VL, et al. Bioconjugated gold nanoparticles as a molecular based contrast agent: implications for imaging of deep tumors using optoacoustic tomography. Molecular Imaging & Biology. 2004;6(5):341-349.
3. Shankar S, Bhargava Sm Sastry M. Synthesis of gold nanospheres and nanotriangles by the Rukevich approach. Nanoscience Nanotechnology. 2005;5:1721-1727
4. Grabar KC, Freeman RG, Hommer MB, Natan J. Preparation and Characterization of Au Colloid Monolayers. Analytical Chemistry. 1995;67:735-743.
5. Nagao O, Harada G, Sugawara et al. Small-Angle X-Ray Scattering Method to Determine the Size Distribution of Gold Nanoparticles Chemisorbed by Thiol Ligands. Japanese Journal of Applied Physics. 2004;43(11A):7742-7746.
6. Haiss W, Thanh NTK, Aveyard J, Fernig DG. Dermination of Size and Concentration of Gold Nanoparticles from Uv-Vis Spectra. Analytical Chemistry. 2007;79:4215-4221.
7. Liu Y, Shipton MK, Ryan J. Synthesis, stability and cellular internalization of gold nanoparticles containing mixed peptide-poly(ethylene glycol) monolayers. Analytical Chemistry. 2007; 79(6): 2221-9.
8. Mukhopadhyay R, Theriault RL, Price JE. Increased levels of alpha6 integrins are associated with the metastatic phenotype of human breast cancer cells. Clin Exp Metastasis. 1999;17:325-332.
9. Lasfargues EY, Coutinho WG, Redfield ES. Isolation of two human tumor epithelial cell lines from solid breast carcinomas. Journal of National Cancer Institute. 1978;61:967-978.

7. Appendices:

"HER2/neu-targeted Gold Nanoparticle contrast agents for Digital Mammography and Digital Breast Tomosynthesis" by Roshan Karunamuni, A THESIS in Bioengineering Presented to the Faculties of the University of Pennsylvania in Partial Fulfillment of the Requirements for the Degree of Master of Science, August 2008.

HER2/neu-targeted Gold Nanoparticle contrast agents for Digital Mammography and Digital Breast Tomosynthesis

Roshan Karunamuni

A THESIS

in Bioengineering

Presented to the Faculties of the University of Pennsylvania in

Partial Fulfillment of the Requirements for the Degree of Master of Science

2008

_____

ANDREW MAIDMENT, PHD

_____

SUSAN MARGULIES, PHD

To Thath, Am, and Ak

ACKNOWLEDGEMENTS

I would like to thank my mentor, Dr. Andrew Maidment for all his help and support over the last year that I have worked with him. His guidance and motivation have helped me discover that graduate school is the best place for me. I would also like to thank Dr. So-Jung Park for help in making the nanoparticles, as well as Dr. Andrew Tsourkas for ideas on how to functionalize them. I would like to thank everyone from the x-ray laboratory: Dr. Predrag Bakic, Dr. Ann-Katherine Carton, Dr. Despina Kontos, Dr. Cuiping Zhang, Dr. Johnny Kuo for all the help and words of advice. In addition, I would like to thank Dr. Anatoliy Popov for teaching me the fundamentals of chemistry, and assisting me with the reactions and experiments. I am very thankful to Dr. Rong Zhou, Dr. Hui Zhang and Karthik Raju for all the help with the cell cultures.

I would also like to thank Dr. Paul Heiney for his help with the SAXS measurements, Dr. Nucleus Xu for the UV/Vis spectra and Dr. Douglas Yates with the TEM readings. I am extremely grateful to Dr. Timothy Zhu for introducing me to the field and helping in so many ways, during my early years. I would also like to thank everyone at the Department of Bioengineering, especially Ms. Kathleen Venit. I would also like to acknowledge that this work was partially supported by the Department of Defense grant W81XWH-06-1-0618, titled “Gold Nanoparticle Contrast Agents in Mammography: A Feasibility Study.”

Finally, I would like to thank my family, to whom I owe so much; my parents, Ananda and Chandrika, and my sister, Ganga, for believing in me when I did not have the fortitude to believe in myself.

TABLE OF CONTENTS

TABLE OF FIGURES

1. Introduction

1.1 Background on Molecular imaging

The development on molecular/functional imaging agents arose from the need for radiologists and surgeons alike to gain more information about the tumors that were being imaged. Traditional imaging techniques provide an anatomical and structural profile of the tumor site, and lend information such as tumor size and diameter, but cannot divulge more of the biological and cellular information of the cancer cells. Information can be garnered such as the efficacy of tumor shrinkage caused by a tumor drug over time, the growth and proliferation rate of the dividing cancer cells, and the presence of biomarkers, both physical (proteins on the surface of the cell) and chemical (activation of genes). The answer to these questions is thought to lie with the development of functional imaging agents. These molecules would report from the scene of cellular events, and could give a direct observable response to cellular activity. Molecular imaging thus makes molecular processes visible, quantifiable and traceable over time in patients, and provides in-depth information on the functional and cellular activity of the tumor cells. The current trend in imaging research is to provide a sense of both the structural and functional characteristics of the tumor tissue in the same image. This is achieved by, either the fusion of different modalities or the development of appropriate contrast agents for a more self-contained system.

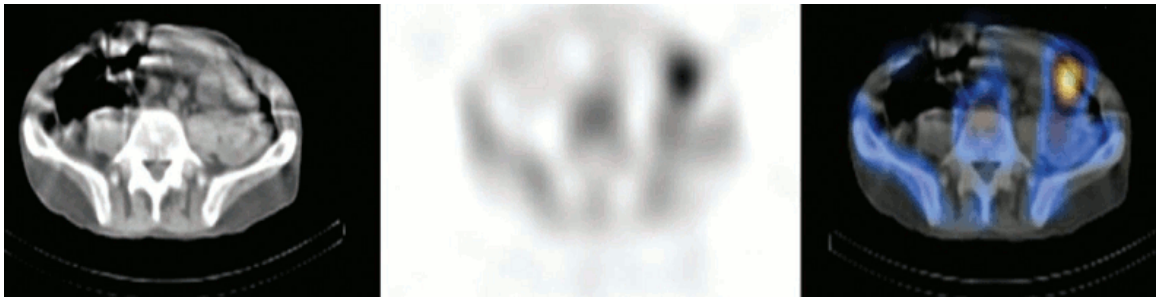

Figure 1. SPECT/CT fusion images in a patient with newly diagnosed abdominal T-cell non-Hodgkin's lymphoma and increased uptake of Ga-67 in left pelvis. CT(left), SPECT (center) and SPECT/CT (right) images are shown. Obtained from Keidar et al. [1]

1.2 Current research in developing molecular imaging agents

Much of the recent interest in the development of molecular imaging agents has been directed towards implementation with modalities such as positron emission tomography (PET), single photon emission computed tomography/computed tomography (SPECT/CT) and magnetic resonance imaging (MRI) [2, 3].

Currently, the most popular molecular imaging agent used in PET is the glucose analog ^{18}F-fluoro-2-deoxy-D-glucose (F-FDG) [4-6]. Tumors are constantly dividing, and thus require an elevated uptake of glucose to fuel their internal cell machinery. This results in FDG being accumulated more in tumor cells than benign cells [5]. The differential uptake of the imaging agent between the tumor and normal cells is what allows us to accurately determine which cells are cancer cells. This agent therefore provides a unique insight into the level of glucose metabolism, and consequently cell proliferation, of the tumor cells. This information can be used to better characterize the tumors *in vivo* as well as improve the monitoring of the cancer therapy response. The agent, coupled with a radioactive tracer molecule, will be able to determine, within days, whether a particular course of therapy is working [7]. However, F-FDG induces a considerable amount of background signal, since there are many benign cells in the body

that uptake large quantities of glucose, such as the heart muscle or areas of natural inflammation [4]. This has fueled the research for a more targeted contrast agent that will only interact with the required tissue.

One example of such a novel targeted agent, Pittsburg Compound-B (C-PIB) has been approved for use in Alzheimer's patients as a PET probe [8]. C-PIB is a thioflavin derivative that at radiotracer concentrations has a high affinity for fibrillar Aβ, a pathological hallmark of Alzheimer disease (AD) [9]. C-PIB is therefore able to more clearly distinguish between benign cells and tissue that is of interest to the physician. Researchers have found that the increased uptake of the tracer may indicate the presence of early Alzheimer's disease in patients suffering from mild cognitive impairment (MCI) [10]. Studies have also shown that the agent can be used to differentiate between AD and front-temporal lobar degeneration (FTLD) [8]. The diseases have overlapping syndromes and neurological profiles, with many of the pathologically proven FTLD cases meeting the clinical criteria for AD. Accurate discrimination between these two diseases has very promising implications for positive prognosis in patients.

The most popular imaging agents used in MRI are gadolinium-based agents [11]. The gadolinium is administered with a chelating agent such as diethylenetriamine penta-acetic acid (DTPA) to provide a biocompatible surface for use *in vivo* [11]. Recent advances in the imaging agent have been directed towards more targeted association of the gadolinium compounds with tumor tissue. Alerion have worked on targeted biochemically activated contrast agents [12]. These agents possess chemical caps that prevent the interaction of the imaging agent with water molecules in the body. A target recognition element is activated once the agent has reached the target, and the blocking

agent is removed, activating the gadolinium and generating a detectable magnetic resonance signal. Another promising avenue is the synthesis of ultra-small supermagnetic iron oxide particles; small particles of ferrite that can be used as a paramagnetic contrast agent in MR imaging [13] . Iron-oxide particle-enhanced MRI has been used as a measure of the liposome enrichment in tumor tissue [14]. These probes have also been used to track immune-stimulating cells implanted into cancer patients for treatment purposes. Targeted contrast agents will allow for fewer repeated injections, meaning that imaging periods can be extended without discomfort to the patient.

Gallium-67 has been used in conjunction with co-registered SPECT/ CT images to localize inflammation and infection [1, 11]. The fusion of both anatomical and functional imaging techniques presents far greater information that could be provided by each alone. The functional imaging aspect shows areas of increased blood flow, and increased vascular membrane permeability whereas the superior spatial resolution of the anatomical image will result in excellent tumor localization and characterization. The limitations of each system are offset by the benefits of the other, resulting in more information on the tumor being readily available. Figure 2 shows such an example, where the combination of CT and gallium-enhanced SPECT imaging can be used to phenotype the different areas of the rodent heart [15]. There has also been work done in the physical development of an imaging system that combines the acquisition of both the PET and CT images in a single run. This form of simultaneous data acquisition minimizes temporal and spatial mismatches between the two images [16].

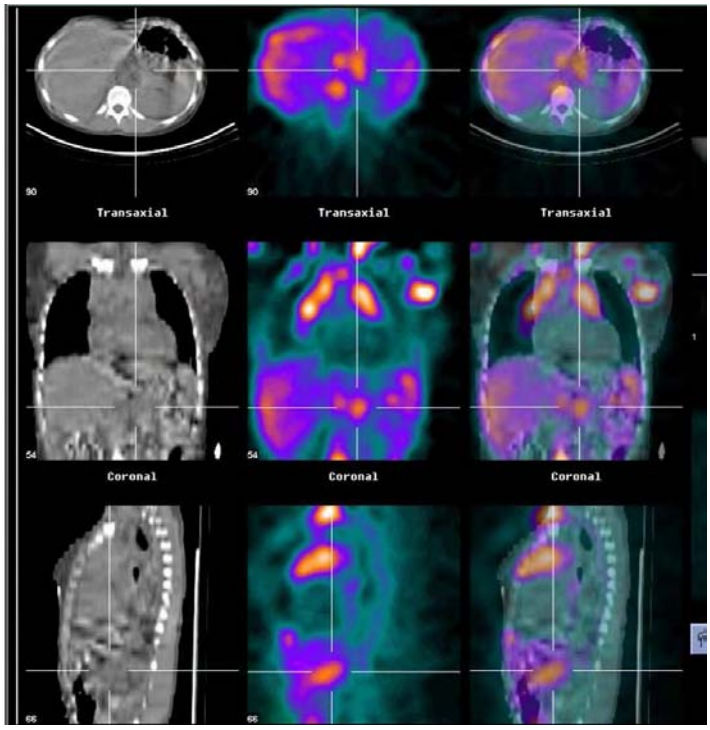

Figure 2. Co-registered CT and gallium-enhanced SPECT obtained from Badea et al. [15]

CT contrast agents consist of typically either iodine, or barium sulfate and are considered to be blood-flow or blood-pool agents [17]. These substances attempt to highlight the flow of blood through vessels in the body to enhance the structures of organs such as the brain, liver or kidney. The agents are often injected intravenously into the patient, and work by substantially attenuating the x-ray beam compared to bone or tissue. The agent is finally removed from the blood stream by a combination of the liver and kidney. The mechanism of action of the iodinated contrast agents using in x-ray imaging is further discussed in the following section.

1.3 Current molecular imaging agents for use with breast imaging

The development of x-ray contrast agents is thought to have started as early as 1895, in the same year in which x rays were discovered [18]. X-ray contrast agents, as used today, permit visualization of the details of internal structures that could not be otherwise assessed. Currently the most commonly used vascular x-ray imaging agents are

formulated with iodine-based compounds. These molecules are typically small tri-iodobenzene compounds with several added substitutions for improved water solubility [18]. Iodinated x-ray contrast agents are very stable and chemically inert, resisting biological degradation *in vivo* over long periods of time. Iodine has a relatively high x-ray attenuation coefficient compared to soft tissue which allows for easy differentiation when imaged with x rays [18].

These agents make use of the fact that tumor tissues often possess disorganized vascular networks which allow for the permeation of molecules from the blood vessels to the tumor tissue [17, 19, 20]. Solid tumors must often induce angiogenesis for the production of a new blood supply network, in order to maintain the required nutrient and oxygen levels needed for their rapid growth and cell division [20]. These vessels are generally considered to be anatomically heterogeneous structures. They consist of relatively undifferentiated channels, lined by simple endothelium and fewer pericytes and smooth muscle cells than would be expected of comparably-sized vessels in normal tissues [19]. Because of this poor structure, tumor vessels are more permeable to circulating macromolecules than those found in benign tissues. Iodinated-contrast agents can therefore easily diffuse across the newly-formed blood vessels that supply the tumor, and accumulate within, and around the tumor site.

Iodinated-contrast agents do, however, possess several limitations that have fueled the research for improved x-ray imaging agents. The non-specific nature of the contrast agent results in random vascular permeation, and its relatively low molecular weight facilitates rapid renal clearance, which in turn necessitates shorter imaging times [21]. Intra-arterial catheterization is often required, and carries with it the risks of arterial

puncture, dislodgement of plaque, stroke, myocardial infraction, anaphylactic shock and renal failure [21]. Because these agents lack the appropriate layer of surface biomolecules to prevent the non-specific binding of blood serum proteins, the percentage of the injected dose that reaches the tumor site is low, meaning that large concentrations and amounts of the agent are often needed to produce a detectable signal [21].

1.4 Breast imaging modalities

X-ray imaging techniques, breast CT, digital mammography (DM) and digital breast tomosynthesis (DBT), combined with contrast agents have been shown to demonstrate enhancement of breast cancers and significantly increase lesion conspicuity [22].

Breast CT was first studied in the 1970's and coincided with the development of the CT technology [23]. Boone *et al.* have successfully designed a dedicated breast CT system capable of cone-beam CT of the breast [24]. The system is capable of producing a fully tomographic image of the breast that can be used either for screening of patients or for diagnostic purposes. Boone found that masses were significantly more conspicuous on breast CT images compared to film-screen mammography [23]. There was no observed difference in the conspicuity of benign or malignant lesions with the two types of images, although women with denser breasts did tend to have lesions that were not as visible when imaged with the breast CT system [23]. Breast CT also appeared to suffer in the identification of microcalcification lesions, an area in which mammography performed markedly better [23]. Chang *et al.* have studied contrast-enhanced breast CT in 67 patients and were clearly able to distinguish between benign and malignant tissues[25] . There is , however, a high radiation dose to the breast and the system is often limited by the spatial resolution.

Contrast-enhanced digital mammography (CE-DM) has been developed by a number of groups around the world, and has been shown to better identify and characterize lesions in the breast [25]. Jong *et al*. have studied and reported their initial clinical findings with CE-DM using Omnipaque 300 as an intravascular contrast agent. Enhancement was observed in 89% of all invasive cancers, while only 42% of the benign lesions that were initially deemed troublesome by mammography showed significant contrast uptake [25]. They also found that CE-DM was superior in the identification of mammographically dense breast when compared to standard film-screen mammography [25]. CE-DM is also relatively inexpensive when compared with current MR technology and will thus, be more readily available at more locations.

However, the superimposition of breast tissues that result as a consequence of the projection technique of DM may unfavorably impact lesion conspicuity. Digital breast tomosynthesis (DBT) is a novel x ray imaging method in which sequential tomographic images through the breast can be reconstructed using a limited number of projection images acquired at various angles [22]. The technique attempts to overcome the superimposition of tissues seen with 2-D breast imaging techniques such as DM, and increase both lesions conspicuity and localization. Rafferty *et al* have claimed a 16% increase in sensitivity and an 85% decrease in the rate of false positives with DBT when compared to DM [22].

Contrast-enhanced DBT (CE-DBT) has been pioneered at the University of Pennsylvania, using iodinated contrast agents. A quantitative evaluation of the contrast uptake is easily computed because of the linear relationship between attenuation and contrast concentration [22]. Chen *et al.* have reported that CE-DBT demonstrated

vascular characteristics of breast lesions that were consistent with information provided by MR in all 13 cases studied [22]. They concluded that CE-DBT had the potential to be a relatively low-cost alternative for functional breast imaging that could be applied towards the evaluation of harmful and benign breast lesions. The system is able to provide both accurate breast lesion morphology as well as functional characterization.

1.5 Rationale and Objectives

The goal of this research is to develop bioconjugated gold nanoparticles (AuNP) to be used as molecular contrast agents with DBT and digital mammography. The AuNPs were designed to accumulate within the cytoplasm of tumor cells in high enough concentrations to be visualized using x rays. The AuNPs were targeted to solely interact with those cells that possess a chosen cancer biomarker on the cell surface. Gold has a higher atomic number and a higher absorption coefficient than iodine, resulting in a roughly 3 times greater contrast per unit weight at typical mammographic energies (15 – 40 keV, Figure 3) [21]. Gold is also relatively inert in the body with injections of 10 mg/ml Au in mice showing no signs of toxicity 11 and 30 days after injection [21]. Gold nanoparticles have also been shown to clear the blood more slowly than iodine agents, thus allowing for longer imaging times [21].

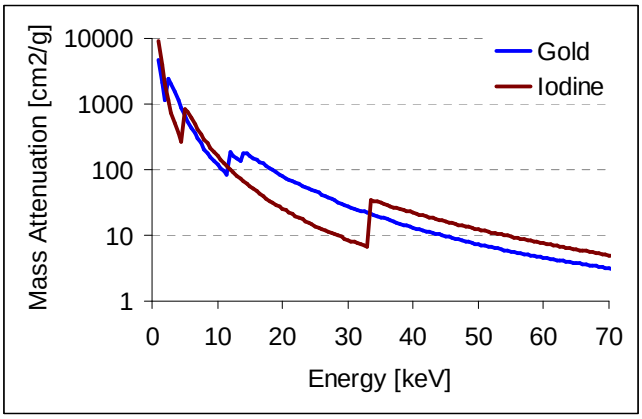

Figure 3. Mass attenuation coefficients for gold and iodine

AuNPs have sparked a considerable amount of interest in the scientific community. This was motivated primarily by their unique optical properties at the near infrared wavelengths, as well as their ease of synthesis and functionalization. Tkachenko has used a AuNP platform for a nuclear targeting mechanism [26, 27]. The 20 nm AuNPs were conjugated to various peptides that serve to induce receptor-mediated endocytosis (RME), interact with the nuclear pore complex and enter the nucleus. The peptide-nanoparticle complexes were then incubated with HepG2 cells and imaged using video-enhanced difference interference contrast (DIC) microscopy (Figure 4).

Figure 4. HepG2 cells incubated with gold nanoparticles imaged with VE-DIC. Obtained from Tkachenko et al. [27]

Moses *et al.* have attached strands of antisense DNA to AuNPs that have the ability to suppress the production of proteins needed by cancer cells to proliferate [28] . Gold nanorods that have been internalized by cancer cells can also be used as therapeutic agents, as continuous exposure to red laser at 800nm results in the photo-thermal destruction of these cells [29]. Niidome *et al.* have developed PEG-modified gold nanorods that have sufficient stealth characteristics *in vivo* to largely escape uptake by macrophages for the imaging of target sites using near-infrared light-scattering or photothermal therapy using near-infrared laser light [29, 30]. Hainfield *et al.* have studied

the possible therapeutic benefits of the select cellular internalization of gold nanoparticles by tumor cells [21, 31]. They have estimated that such cancer cells would receive a significantly larger dose compared to normal tissue during a course of radiotherapy treatment. This work has encouraged us to develop bioconjugated AuNPs as targeted molecular-imaging contrast agents for DM and DBT.

2. Methods

The methodology presented herewith includes the synthesis of the AuNPs, the functionalization of the nanoparticles with a surfactant (surface stabilizing agent) and targeting ligand, and the techniques used to characterize the size, shape, and composition of the AuNPs. The AuNPs are conjugated with an affinity ligand in order to direct the particles to the cancer cells (see Figure 5). The ligand targets a cell surface receptor that is over-expressed in breast cancer cells, and will allow the nanoparticles to discriminate between tumor and benign tissue. Since many molecular contrast agents are limited by their circulation time *in vivo*, a surface stabilizing agent (Figure 5) was added to the nanoparticles to improve their viability in high ionic strength media, such as PBS or blood serum as well as enhance their stealth characteristics in the body. This will ensure that a sufficient number of these particles will reach the tumor and cause a differential attenuation of the x-ray beam.

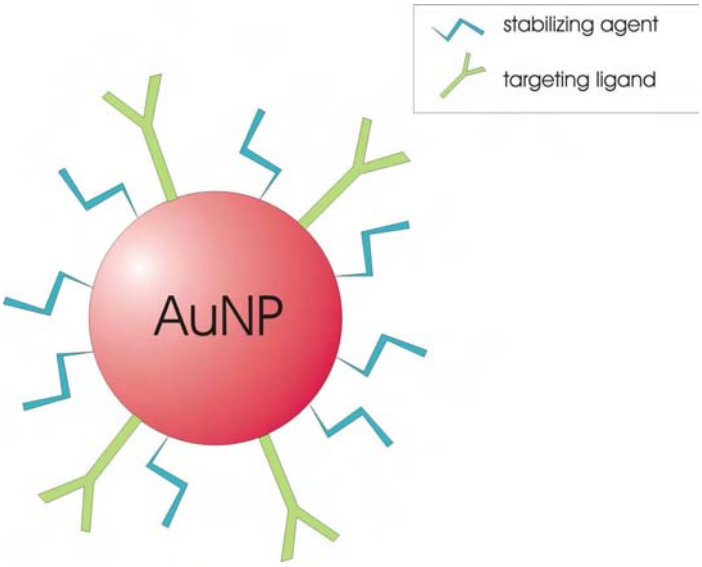

Figure 5. Multi-functionalized AuNP with targeting ligand and stabilizing agent

2.1 Synthesis and Functionalization of AuNPs

2.1.1 Synthesis of AuNP

There exist several approaches for the synthesis of colloidal gold nanoparticles in solution; the majority of which involve the reduction of a gold salt in the presence of a surfactant, or surface-stabilizing agent [21, 32-34]. The choice of reducing agent and surfactant directly impacts the characteristics of the final AuNP solution. Turkevich developed a single phase, water-based method using reduction by citrate at 100 °C to synthesize spherical AuNP with tightly-controlled dimensions [32]. Others have used gold particle seeds introduced into a solution of absorbic acid and cetyltrimethylammonium bromide (CTAB) to develop crystallographically oriented gold nanorods [32]. UV light has been used in some cases, in place of heating the gold solutions, in order to promote particle growth [32]. Careful variation of the parameters of each method can be used to produce AuNPs of varying size, shapes and distributions.

We have used the citrate reduction method, first proposed by Turkevich and extensively refined since, to synthesize our AuNPs. The method is easy to implement, and produces almost spherical particles over a large range of tunable sizes. It is also the most commonly applied method in the field today, whose mechanics (kinetics, stabilization, and environmental dependencies) have been extensively studied. The method involves the reduction of a boiling solution of gold aurochlorate, by citrate, which serves as both the reducing agent and surfactant. The pH and temperature distribution of the gold salt solution at boiling, can affect the morphology of the AuNPs produced. Careful control of these environmental conditions is needed to obtain specific size-defined particles.

The formation of the AuNPs can be broken down into a series of steps. Initially, gold atoms are fused together to form clusters that are evenly distributed throughout the liquid [32]. Gradually, the clusters are coalesced together to form nanoparticles that continue to grow by adding onto their surface the reduced gold present in the solution. The AuNPs are stabilized by absorbing a layer of citrate anions onto their surface [32]. The citrate anions form a protective barrier around the AuNPs and prevent separate particles from fusing together. A higher concentration of citrate anions means that smaller particles are more rapidly stabilized, whereas lower concentrations results in aggregation of growing gold particles and the formation of larger nanoparticles [32]. Larger particles therefore tend to be irregularly shaped, with varied sizes and morphologies. Increasing the initial concentration of gold atoms present in the solution also results in larger AuNPs being produced, as the growing nanoparticles are able to absorb from a larger reservoir of gold atoms in the solution before being passivated by the citrate anions.

Since we require that the AuNPs accumulate within the cytoplasm of tumoregenic cells, we will focus on the range of sizes that allow for the most efficient uptake. AuNPs are taken up by cells through cell-mediated endocytosis and accumulate in vesicles within the cytoplasm. Chithrani *et al.* have shown that AuNPs in the range from 14 to 50 nm are the most densely taken up by mammalian cells (Figure 6), with increased uptake coinciding with increased nanoparticles size [35]. There appears to be a tradeoff, however, between increased cell penetration and increased clearance of the nanoparticles from circulation within the body. Larger AuNPs are more readily removed from the blood stream by macrophages and are more likely to accumulate in the spleen and liver

than smaller particles [35]. Our long term plan is to study the optimal size of AuNP needed to selectively accumulate within the tumor cells, as well as in sufficient quantity to show a reasonable contrast against the background.

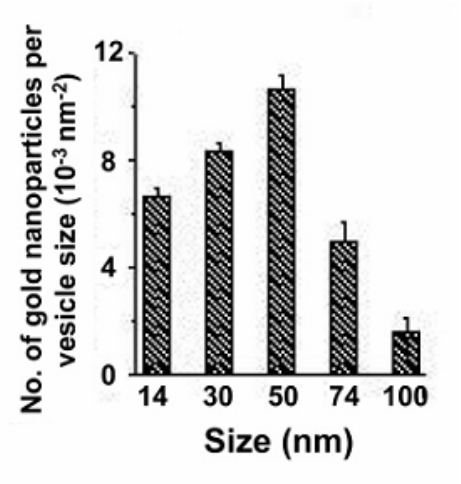

Figure 6. Affect of size of AuNP on uptake my mammalian cells. Obtained from Chithrani et al. [35]

For synthesis of the AuNP, we used the procedure set forth by Grabar *et al.* [36] to synthesize AuNP with an expected diameter in the range of 14 nm using a molar ratio of 4:1 between the gold salt and the citrate. The entire procedure is conducted under a fume hood, and all glassware used was first treated with a solution of aqua regia and promptly rinsed with deionized water. The aqua regia solution consisted of 3 parts 70% nitric acid to 1 part 36% hydrochloric acid. Next, 0.20g of gold (III) chloride trihydrate (Sigma-Aldrich, Missouri, $HAuCl_4.3H_2O$, MW = 393.83) was dissolved with 500ml of triple-distilled water in a 1L round-bottom flask to which a Teflon-coated magnetic stir bar was added. The flask was then placed atop a heating mantle and magnetic stirrer and the gold solution was brought to a boil. Then, 0.57g of sodium citrate dihydrate (Sigma-Aldrich, Missouri, $C_6H_5Na_3O_7.2H_2O$, MW = 294.10) was dissolved in 50ml of deionized water and added to the boiling gold solution. Heating was continued for an additional 10 minutes after which, the hearing mantle was removed and the solution was

stirred for an extra 15 minutes. The resulting colloidal solution was allowed to cool overnight at room temperature after which it was filtered through a 0.2μm membrane filter. AuNP were then synthesized using citrate to gold ratios of 3:1 and 1:1 using the same procedure described above.

Figure 7. The setup for the synthesis of the citrate-capped AuNP solution. The heating mantle is placed on top of a magnetic stirrer, and a 1L flask is fitted with a distillation column and filter.

2.1.2 Functionalization of AuNP with PEG

Surfactants such as citrate and CTAB act as surface charges repelling the AuNPs from one another, and thus keeping them in solution. The charges however can be screened by high ionic strength media that possess a large number of ambient electrolytes resulting in the AuNPs aggregating out of the solution. The citrate anions also form a relatively weak link with the gold surface which allows us to easily replace the citrate anions with a more biocompatible molecule, such as polyethylene glycol [37].

The major drawback of citrate-capped AuNPs is their inability to remain in solution, and subsequent aggregation in highly electrolytic media such as blood plasma [38]. Aggregation of the AuNPs will result in poor targeting of the tumor and increased clearance from the circulation by the reticuloendothelial system (RES) [38]. Citrate-capped AuNPs are also hindered by their inherent negative surface charge which promotes the non-specific attachment of serum proteins and limits their cell-penetrating potential [38]. Thus, a more biocompatible molecule, polyethylene glycol [37], has been chosen to replace the citrate anions on the AuNP surface [33].

PEG chains bound to the surface of AuNP form coiled, flexible hydrophilic chains that shield the surface of the particle from the surrounding solution [39, 40]. The layer of PEG chains serves to block the nonspecific binding of blood serum proteins, as well as other molecules [39]. Since the mechanism of stabilization is more dependent on the steric hindrance of attachment, and not the electrostatic properties of the PEG molecule, PEG-modified AuNP are more stable in salt media than their citrate-capped counterparts [40]. Li *et al.* have shown PEG-modified AuNP to be stable in even high ionic strength media, with increasing stability for an increased ratio of PEG molecules to nanoparticles [33]. Increasing the length of the PEG chain also seems to favor more stable solutions, but too large of a PEG molecule will hinder the attachment of the affinity ligand. We have chosen to use a PEG molecule with a molecular weight of 5000 Daltons, in order to provide sufficient coverage for the AuNP while not hindering the action of the proposed affibody.

PEG-modified gold nanorods have been shown to exhibit enhanced stealth characteristics and longevity for *in vivo* applications by Niidome [30]. CTAB-stabilized

nanorods were found to accumulate by a substantial proportion in the liver, an hour after injection with minimal distributions in other organs. On the other hand, 54% of the injected dose of PEG-modified gold nanorods was present in the bloodstream 1 hour after administration in mice. PEGylated AuNP will thus be able to reach the tumor site in larger numbers, improving target localization.

We obtained O-[2-(3-Mercaptopropionylamino) ethyl]-O'-methyl polyethylene glycol, (mPEG-thiol, MW = 5000 Da) from Sigma-Aldrich (St Louis, Missouri). The compound is shipped as a powder and is stored under argon at -20°C. The structure is shown in Figure 8, with a methyl group at the distal end, and a thiol (SH) group at the other. The methyl group provides a non-reactive terminal group to prevent non-specific attachment of extraneous molecules. The PEG chain will attach to the AuNP surface through the thiol-gold interaction, which has been extensively studied and shown to be an easy method for conjugation of substances onto gold surfaces.

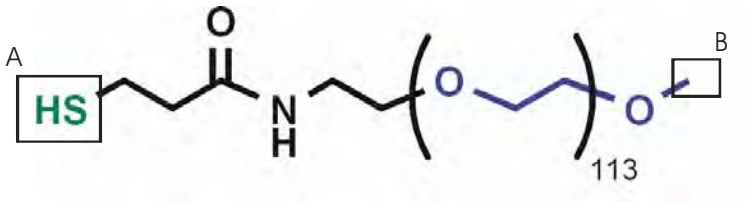

Figure 8. O-[2-(3-Mercaptopropionylamino) ethyl]-O'-methyl polyethylene glycol , with the thiol (A) and the methyl (B) groups labeled

Liu *et al.* have shown, through gel electrophoresis, that increasing the PEG to AuNP ratio beyond 2500:1 results in no increase in the shift of the AuNP. A ratio of 2500:1, with 21nm AuNP, is equivalent to a PEG chain for every 0.5nm^2 on the surface of the AuNP [33]. Sources have indicated that the maximum surface density of PEG molecules on the surface of a AuNP is 1 chain every 7nm^2. By using such a large ratio of PEG to AuNP, we have ensured that there are sufficient PEG chains to completely cover

the surface of the nanoparticles. Any excess PEG chains were removed with centrifugation.

3mL of 21nm AuNP (2.810nM) was mixed with 212μL of 0.5μg/μL PEG-thiol-5000 solution in a 10ml round-bottom flask, and left to be stirred at room temperature for 1 hour. The solution was then centrifuged at 11,400*g* for 26 minutes, and the AuNP pellet was redissolved in 2mL of deionized water after the supernatant had been removed. The resulting AuNP-PEG solution was stored at room temperature.

1ml of each of the newly formed AuNP-PEG conjugates and citrate-capped AuNP was incubated with 3ml of 1% phosphate buffered saline (PBS) solution in order to assess the benefit of the PEG chain in improving the stability of the nanoparticles in salt media. PBS is used as a buffer solution in virtually all cell culture experiments, and possesses an osmolarity and ion concentration that closely matches those of the human body. The reaction of the AuNPs, both conjugated and bare, with the PBS will give us an idea as to how the particles might react *in vivo.*

2.1.3 Multi-functionalization of AuNP with PEG and anti-HER2/neu affibody

In order to direct the AuNP towards the tumor cells, the particles would have to be labeled with an affinity ligand that allows for discrimination between normal and tumorigenic cells. Due to the size of the AuNP and their subsequent inability to penetrate the cell surface membrane into the cytoplasm without additional help, we focused our choice of targets to those that presented themselves in abundance on the cell surface. Cancer cells are rapidly dividing cells, and often express proteins that are essential in cell proliferation and cell activity on the surface of their plasma membrane. Some of the candidate protein targets include transferrin (CD71), MUC1 and HER2/neu receptors. The transferrin receptor is a cell-surface internalizing receptor responsible for almost all

iron uptake in mammalian cells [35, 41]. It is hypothesized that cancer cells overly express this protein in order to meet their iron requirement for increased levels of cell metabolism [42]. It has thus been identified as a possible marker for the proliferation of cancer cells *in vivo*. Overexpression of the transferrin receptor has also been shown to correlate with increased metastatic behavior in rat breast cancer cell types. MUC1 is a mucin glycoprotein that is expressed at base levels in most epithelial cells [43]. It is a transmembrane molecule that is overexpressed in more than 90% of all breast cancers [43]. In normal tissues, the MUC-1 protein is heavily glycosylated with roughly 50 to 90% of its total mass owing to the carbohydrates surrounding the protein structure. In tumor cells, the MUC-1 protein is under-glycosylated leaving an otherwise protected portion of the extracellular region open to targeting [43]. There has been some recent interest in targeting the underglycosylated portion of the MUC-1 tumor antigen for imaging [43].

HER2/neu, also known as ErbB-2 and p185, is an epidermal growth factor receptor protein that is overexpressed in nearly 25-30% of all metastatic breast cancers [44, 45]. It is a transmembrane glycoprotein with an intracellular and extracellular domain. The overexpression of HER2/neu has been associated with aggressively growing tumors, poor prognosis in patients, low rate of disease-free survival, and increased nodal metastases [44-46]. The glycoprotein is known to be involved in the pathways leading to cell growth and cell differentiation [44]. It is also the most widely studied breast cancer marker and an antibody treatment targeting the antigen (Herceptin) has already been approved for use in patients [45]. Information regarding the expression levels of HER2/neu of the most commonly available cancer cell lines is also widely accessible.

Because of the large amount of research conducted on the protein, as well as the ready availability of antibodies targeting it, we have chosen to functionalize our AuNPs to target cells overexpressing HER2/neu.

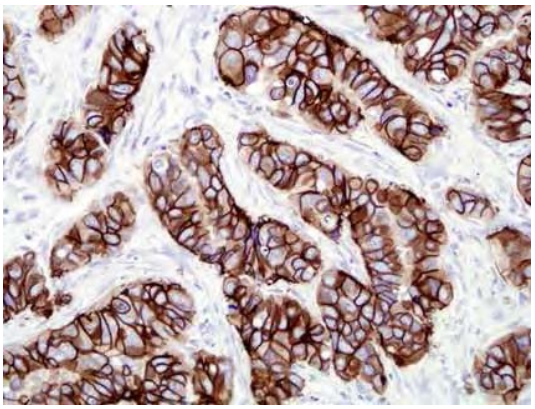

Figure 9. Breast cancer cells that have been stained with a fluorescein-conjugated anti-HER2/neu antibody.

We have obtained an anti-HER2 affinity ligand, from Affibody (Bromma, Sweden), that strongly targets the extracellular domain of the HER2/neu glycoprotein. It is composed of a three-helix bundle based on the scaffold of one of the IgG binding domains of Protein A, a surface protein from the bacterium *Staphylococcus aureus.* The scaffold can be designed to bind with high affinity to the HER2/neu target protein. The affibodies are several times smaller than native antibodies but exactly mimic their function. The anti-HER2/neu affibody molecule is on the order of 14 kDa, while a typical monoclonal antibody has a molecular weight of 150 kDa. The smaller size will allow for easier conjugation onto the AuNP surface and less steric hindrance and influence between affibody molecules on the same AuNP. The affibodies are also able to withstand a broad range of analytical conditions, such as extreme pH and elevated temperatures because of their robust physical nature.

Two varieties of the affibody were obtained: an unconjugated molecule and a fluorescein conjugated molecule. The fluorescein conjugated affibody molecule

possesses a C-terminal maleimide-activated fluorescein reagent for immunostaining protocols with cell cultures. The unconjugated anti-HER2/neu affibody was used for direct conjugation to the surface of the AuNP. The molecule has a C-terminal cysteine amino acid. The thiol side chain of the cysteine molecule will allow for direct conjugation with the AuNP in the same way that the PEG chains are attached. Prior to conjugation, the affibody molecule was first incubated with a solution of 20 mM dithiothreitol (DTT) in order to reduce the disulfide bridges between adjacent C-terminal cysteines and expose the thiol group for attachment. The excess DTT was then removed by centrifugation at 5,000*g* for 5 minutes, and the affibody pellet was resuspended in 1% PBS (phosphate buffered saline) solution.

Multi-functionalization of the AuNP with a mixed monolayer of PEG and anti-HER2/neu affibody was carried out sequentially, in two discrete steps as documented by Liu *et al.* Liu showed that sequentially adding the PEG chain, centrifuging the solution, and then attaching the affinity ligand over adding both components to the AuNP together, vastly improved the stability of the final product in salt solutions. AuNP prepared in this manner using PEG-900 molecules and an antibody resisted aggregation in solutions containing sodium chloride (NaCl) at concentrations in excess of 1M. By comparison, the concentration of NaCl in the 1% PBS solution, in which the citrate-capped AuNP were found to aggregate, is 23 mM. Liu hypothesized that the increased stability from the sequential method stemmed from the kinetics of the attachment. If added together, the affinity ligands, which are generally highly cationic, would associate with the negatively charged citrate-capped AuNP before the PEG molecules had a chance to form a protective barrier, resulting in reduced stability. In our case, it would be impossible to

even consider adding the two components together as the affibody molecule is heavily diluted in PBS for storage, and would cause the citrate-capped AuNP to aggregate upon mixing.

The following protocol was used to multi-functionalize 21 nm AuNP with a mixed monolayer of PEG chains and anti-HER2/neu affibody molecules. 3ml of our 21nm AuNP (concentration is determined in section 3.2.3) was mixed with 170μL of 0.5μg/μL of PEG-thiol solution in a 10ml round-bottom flask, and stirred at room temperature for 1 hour. The solution was then centrifuged at 11,400*g* for 20 minutes, and the resulting pellet was resuspended in 250μL of 1% PBS solution. 85μg of 1mg/mL anti-HER2/neu affibody was then added to the PEGylated AuNP solution. The mixture was stirred for 1 hour at room temperature, and then centrifuged at 11,400*g* for 26 minutes. The AuNP-PEG-affibody pellet was then redissolved in 500μL of PBS.

2.2 Characterization of AuNP solutions

A combination of small angle x-ray scattering (SAXS), transmission electron microscopy (TEM) and UV-Vis spectroscopy was used to determine the size, distribution and concentration of the different AuNP solutions. Each method provides a slightly different quantitative or qualitative characteristic of the AuNP.

2.2.1 TEM images of AuNP

In order to visualize the AuNPs, we have used transmission electron microscopy (TEM) to obtain images of the particles in solution. TEM operates using the same principles as standard bright-field light microscopy, but uses a beam of electrons instead of photons of light to illuminate the specimen [47, 48]. The maximum resolution that can be obtained using light microscopy is limited by both the numerical aperture of the system as well as the wavelength of visible light (400 – 700 nm). TEM overcomes this

limitation by using electrons with much lowers wavelengths, so that structures on the order of a few angstroms (10^{-10} m) can be imaged [48].

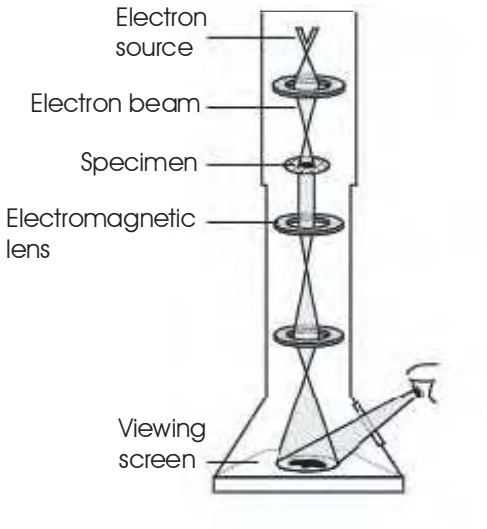

Figure 10. TEM layout. Obtained from [47]

Figure 10 shows the layout of a typical transmission electron microscope [47] . Electrons are generated by thermionic emission from a tungsten filament at the top of the column and accelerated through vacuum by an electrostatic potential to gain the desired energy and required wavelength [47]. The beam of electrons is then focused by electrostatic and electromagnetic lenses through the specimen that is being studied [48]. Electron-dense materials, such as gold, interact with the electron beam and scatter the electrons out of the path, forming a shadow of the specimen on the final image. The transmitted beam contains information about electron density and phase that can be used to recreate the image of the specimen.

For our experiments, a drop of the AuNP solution was placed on a carbon grid and allowed to dry for 6 hours prior to imaging. The grid was then imaged using a JEOL 2010F (Gaton, Pleasanton, CA) high-resolution TEM which has a point-to-point resolution of 0.23 nm. The citrate-capped AuNP and PEG-conjugated AuNP were both

imaged using a beam energy of 76 keV. Multiple images of each sample were obtained in order to obtain the size dispersion and homogeneity of the sample.

The microscope also has analytical capabilities to determine the chemical composition of the specimen. This is performed by introducing an x-ray detector close to the specimen while it is being irradiated by the electron beam and recording the characteristic radiation emitted from the sample. When an atom is bombarded by electrons, some of the electrons are knocked out of their shells in a process called inner-shell ionization. The vacancy is then filled by an electron from an outer-shell by self-ionization (Figure 11). These outer-shell electrons are more-loosely bound than those that are ejected and so the atom contains excess energy. For heavy elements, such as gold, this energy is emitted as a photon with characteristic radiation energy equal to the difference in binding energies between the outer-shell and ejected electron. This characteristic radiation is unique to the element, and varies with the type of shell transition. By recording the characteristic photons emitted by the specimen, the elements present within the sample can be ascertained.

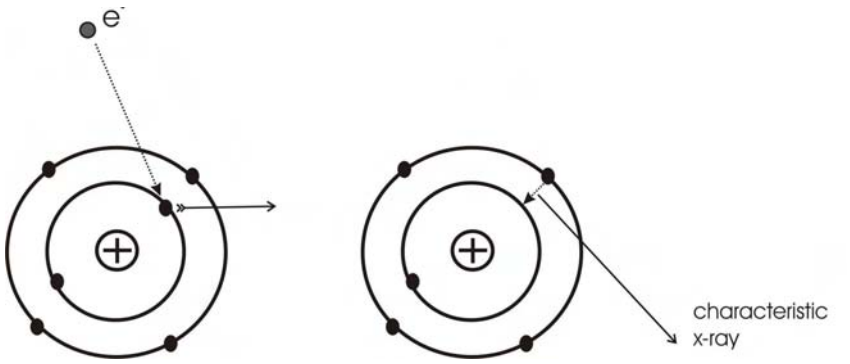

Figure 11. Schematic of inner-shell ionization, and the production of a characteristic x ray

2.2.2 SAXS measurements

SAXS records the elastic scattering of x rays by a sample at very low angles, typically in the range from 0.1 to 10° [49]. Colloidal solutions consist of macromolecular particles that are typically much larger than the surrounding solvent molecules, but still small enough to follow a random Brownian-type motion. By focusing a low divergence x-ray beam (Figure 12) into a colloidal solution and observing the coherent scattering pattern that arises from the electron density inhomegenities within the sample, information about the macromolecules present can be obtained [50]. Because gold has a much larger electron density than the surrounding solution of water, this technique is especially useful for determining the diameter and the size dispersion of the AuNPs. Whereas TEM can only provide an estimation of the diameter of each AuNP, SAXS provides a quantitative analysis of the size distribution for an entire sample.

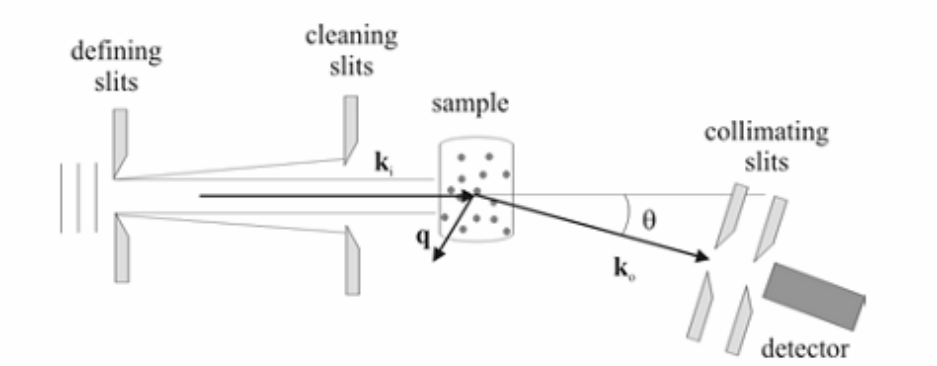

Figure 12. Standard setup for SAXS measurements of colloidal solutions. Obtained from Diaz et al. [49]

A brief description of the principles of SAXS is described here [50]. The x-ray scattering vector *q* is defined by

$$|\boldsymbol{q}| = q = \frac{4\pi \sin(2\theta/2)}{\lambda} \quad (1),$$

where 2θ is the scattering angle and λ is the wavelength of the incident radiation. The intensity of the scattered beam of x-rays passing through the sample is measured at different values of *q* and is recorded at the detector. The intensity ***I(q)***, of the small-angle x-ray scattering caused by a scattered is given by,

$$I(\boldsymbol{q}) = |F(\boldsymbol{q})|^2,\ F(\boldsymbol{q}) = \int_V \Delta\rho(r)e^{i\boldsymbol{q}\cdot r}dV \quad (2),$$

where F(***q***) is the form factor, obtained by integrating the product of $\Delta\rho$,the difference in the electron densities between the scatterer (AuNP) and the matrix (water) and $e^{i\boldsymbol{q}\cdot r}$, the amplitude of the scattering at a distance *r*. The equation for the form factor can be approximated, in the case that the scatterer is a sphere with a diameter D_0 into

$$F(\boldsymbol{q}) = \frac{4\pi}{q^3}[\sin(\frac{qD_0}{2}) - \frac{qD_0}{2}\cos(\frac{qD_0}{2})] \quad (3).$$

It can be seen that the form factor does then vary with the diameter of the scattering particle for a given scattering vector, and scattering angle. A library of the intensities of the scattered beams for different sized particles can then be calculated, for a specific range of values of the scattering vector.

The sample is prepared as follows. 1 ml of the aqueous AuNP is placed in a plastic cuvette and sealed with quick-drying epoxy. The cuvette is then placed in the path of the x-ray beam under vacuum, and the intensity of the scattered beam is measured at different scattering angles. The resulting dataset is compared against the library of scattering intensities to approximate the diameter of the AuNP, assuming a certain distribution. 1 ml of water was also placed in a cuvette, and then the scattered beam measured in order to determine the background scattering present within the sample of the AuNP. The intensity plot can thus be subtracted for this background radiation, and a

more accurate measurement of the diameter of the AuNP and size dispersion can be obtained. SAXS analysis was conducted for the AuNP that were synthesized using a molar ratio of 4:1 between the citrate and the gold salt to confirm that the nanoparticles were 14 nm in diameter.

2.2.3 UV-Vis spectroscopy analysis

AuNP, like most metal nanoparticles, are interesting in the fact that their optical properties depend strongly upon the particle size and shape. Bulk gold looks yellow whereas thin Au films appear blue in transmission and the color gradually changes through orange and purple to red when the size of the AuNP is reduced to 3 nm. The light absorption by AuNP, like most other metal nanoparticles, is the result of the coherent oscillation of free conduction electrons in response to the alternating electric field of an incident electromagnetic field [51]. When a small spherical AuNP is irradiated by light, the electric field of the incoming radiation causes the electron cloud to be displaced, resulting in a temporary dipole in the AuNP [52]. A restoring force, from the Coulombic attraction between the displaced electrons and the nuclei, attempts to compensate for this, resulting in the oscillation of the electron cloud relative to the nuclei at a resonant wavelength [52]. The wavelengths of light absorption that produce these plasmon oscillations are referred to as surface plasmon resonance (SPR) bands. The oscillation wavelength is influenced by the size and shape of the particle, the dielectric properties of the surrounding media, and the surfactants and other molecules present on the surface of the AuNP [52].

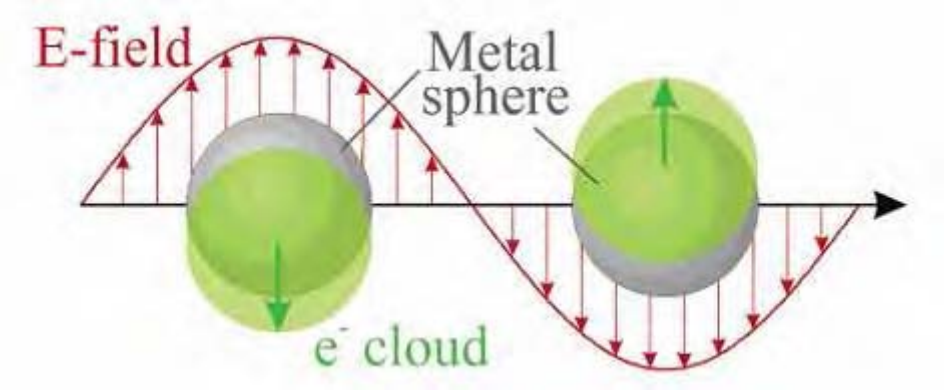

Figure 13. The displacement of the electron cloud relative to the nuclei upon interaction with an electromagnetic field. Obtained from Kelly et al. [52]

Haiss *et al.* [51] have shown that as the diameter of the AuNP increases, the peak wavelength of the surface plasmon band increases. The relationship is not linear, but can be approximated in the range from 5 to 80 nm, provided the AuNP are suspended in deionized water. The typical SPR peak for AuNP with diameters in the range from 15 to 100 nm is typically between 520 and 580 nm. This is in the ultraviolet-visible range of light, and so a UV-Vis spectrophotometer must be used in order to obtain the absorbance spectrum of the AuNP. A 1 ml sample of AuNPs is placed in a reduced-volume cuvette, and then examined using a Perkin Elmer, Lambda 20 UV/Vis Spectrometer. The absorbance of the sample is scanned from 350 to 800 nm, using data intervals of 1 nm. This extended range allows us to examine any possible effects of aggregation or conjugation of biomolecules onto the AuNP surface. Absorption spectra were obtained for each of the citrate-capped AuNP, PEGylated AuNP, and multi-functionalized AuNP. We investigated the effect of conjugation of biomolecules to the AuNP surface on the peak wavelength of the SPR band.

The mathematical relationship between the peak wavelength of the SPR band and the diameter of the AuNP has been researched but is not widely reported as there are other more direct means of determining the size of the AuNP. Instead, the absorption

spectrum of the AuNP has been used in determining the concentration of the AuNP using extinction coefficients. The extinction coefficient is defined as the fraction of light lost to scattering and absorption per unit distance of a particular chemical species at a given wavelength. It is an intrinsic property of that species, and depends on the concentration of the species [51]. The formula is given by

$$\varepsilon_\lambda = A_\lambda / c \quad (4),$$

where ε_λ is the extinction coefficient of the species at a wavelength λ; A_λ is the absorbance of light at that wavelength and c is the concentration of the species in the sample. Haiss *et al.* have compiled a table of AuNPs with different diameters and their corresponding extinction coefficients at a wavelength of 450 nm. The absorbance of the AuNP sample at 450 nm will provide us with the concentration of the AuNP in moles per liter (molar).

3. Results

3.1 Synthesis of AuNPs

Upon addition of the sodium citrate solution, the yellowish gold solution first turned colorless and then to a burgundy-red. The final color of the AuNP solution depended on the molar ratio of citrate to gold that was used (Figure 14). The AuNPs produced using a 4:1 ratio remained a light burgundy, whereas those synthesized with a 3:1 ratio were more purple-red. Finally, the particles produced using the lowest citrate to gold ratio of 1:1, were dark brown-purple.

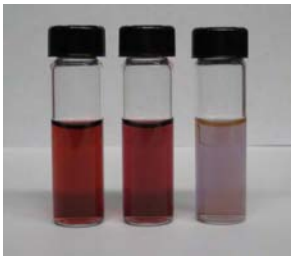

Figure 14. Colloidal AuNP synthesized using molar ratios of 4:1 (left), 3:1 (center) and 1:1 (right)

All of the nanoparticle solutions were stable at room temperature, although those produced with a 1:1 gold ratio did tend to habitually coalesce at the bottom of the glass container. These particles also could not be filtered through a 0.2μm membrane filter, as this appeared to remove all particles from the solution leaving only water.

3.2 Characterization of AuNP solutions

3.2.1 SAXS analysis of AuNPs

SAXS analysis was performed for both the 4:1 AuNP solution as well as a solution of pure water to gauge the effects of the solvent on the scattering properties of the particles. Measurements for both samples were taken over the course of 1 hour. Shown in Figure 15, are the false-color images obtained for the AuNP (a) and water (b) solutions.

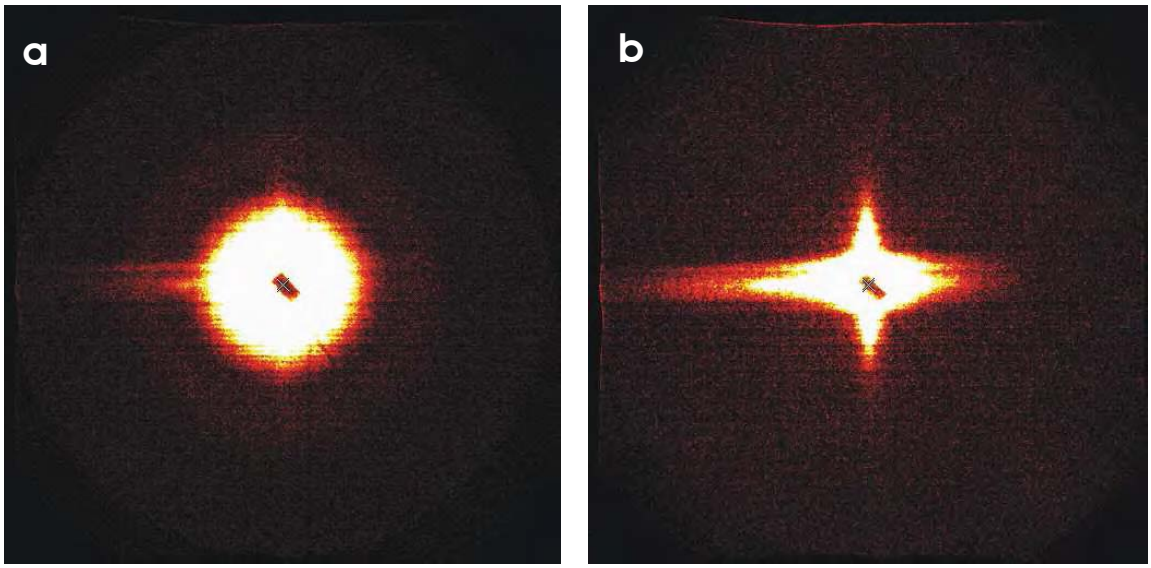

Figure 15. False-color SAXS images of AuNP (a) and water (b) solutions

The image of the nanoparticles shows a secondary ring around the central peak, very similar to a 2-dimensional *sinc* function. In contrast, the water solution shows a steady decay of the intensity of the scattered beam from the central peak. This secondary ring is essential in obtaining the diameter of the particles, as much of the information available from SAXS is present in this ring.

The logarithm of the intensity of the scattered beam is plotted against the scattering vector q for the water solution (Figure 16). The intensity was then fitted to a polynomial (close to linear) plus a $1/q^4$ function, which described, within reasonable error, the scattering profile of water in the system.

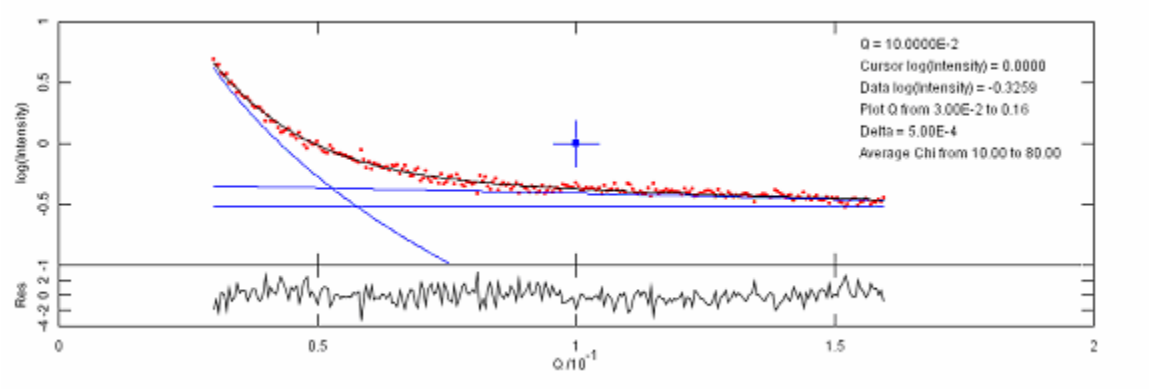

Figure 16. Scattering profile of water, fitted to a polynomial and $1/q^4$ (shown in blue)

The scattering profile was then obtained for the solution of AuNPs. The logarithm of the intensity was fitted to a Rayleigh function, a linear background plus a $1/q^4$ function. The linear and $1/q^4$ components both arise from the water solvent and it is the Rayleigh function that describes the scattering intensity of the AuNPs. Table 1 shows the parameters of the different types of functions used to approximate the intensity function over the range of values of q. The Rayleigh function provides the radius of the scattering particle (AuNP) in angstroms, 69.81, which corresponds to a diameter of roughly 14 nm.

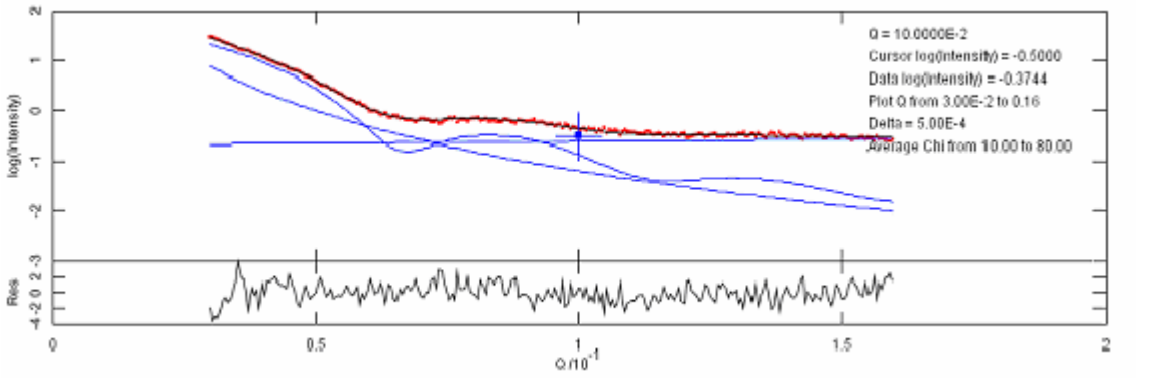

Figure 17. Scattering profile of AuNPs, fitted to Rayleigh function, background plus $1/q^4$.

Table 1. Functions used to approximate the scattering intensity function, and their values

Name	Polynomial (Linear)	Rayleigh (radius in nm)	Power (amplitude)
Value	0.31	6.98	5.73E-06
Standard Error	6.032 E-2	6.60 E-03	8.04E-08
Lower Limit	0.18	6.95	5.13E-06
Upper Limit	0.43	7.01	6.30E-06

The 14 nm obtained for the AuNPs synthesized using a 4:1 ratio between the citrate and gold precursor concurred with the results obtained by Grabar, whose method we implemented.

3.2.2 TEM images of AuNP solutions

Figure 18 shows some of the images obtained from imaging the citrate-capped AuNPs synthesized using a citrate to gold ratio of 3:1.

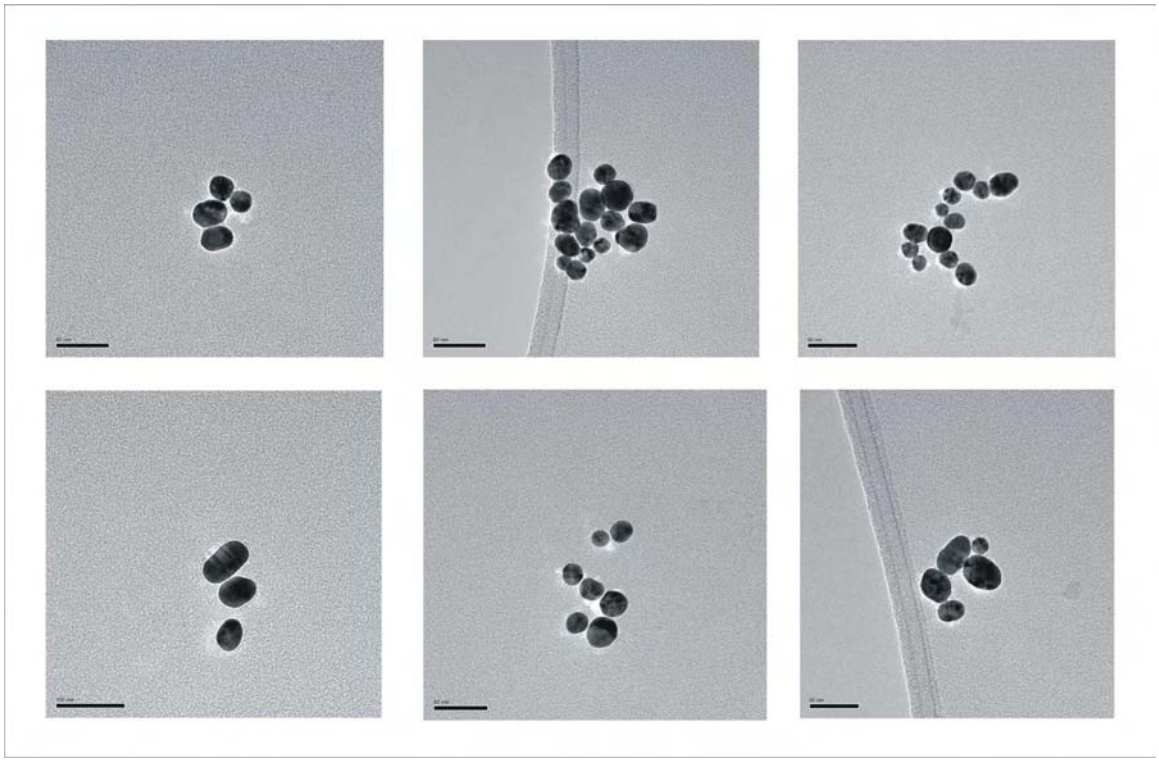

Figure 18. TEM images of citrate-capped AuNP

The average diameter of the AuNPs was found to be 21 nm. The particles were all spherical in shape and many of them were found to have clumped together. This is thought to be because of the weak stabilizing force of the citrate anions on the AuNP surface. The repulsive force between the negatively charged AuNP is not sufficient to prevent clumping of the particles on the carbon grid.

There exists a little inhomegenuity in the size of the nanoparticles, with some particles larger than others. The diameters of the AuNPs were measured using ImageJ, and a summary of the results is presented in Table 2.

Table 2. The size distribution of 47 AuNP imaged through TEM

Mean Diameter (nm)	Standard Deviation	Min	Max
21.3	4.2	13.4	30.2

A tighter control of the temperature distribution of the solution during synthesis of the particles may have resulted in a more homogeneous particle distribution.

Gold crystals are structured as a face-centered lattice, and the atoms are arranged in regular arrays that are spaced an equal distance apart [53]. This is illustrated in Figure 19 that shows a magnified view of a AuNP. A line-plot of the intensities through the crystalline pattern shows that the peaks are spaced roughly 2 Angstroms (0.2 nm) from each other. These findings agreed with findings presented in the literature regarding the growth and structure of gold crystals [53].

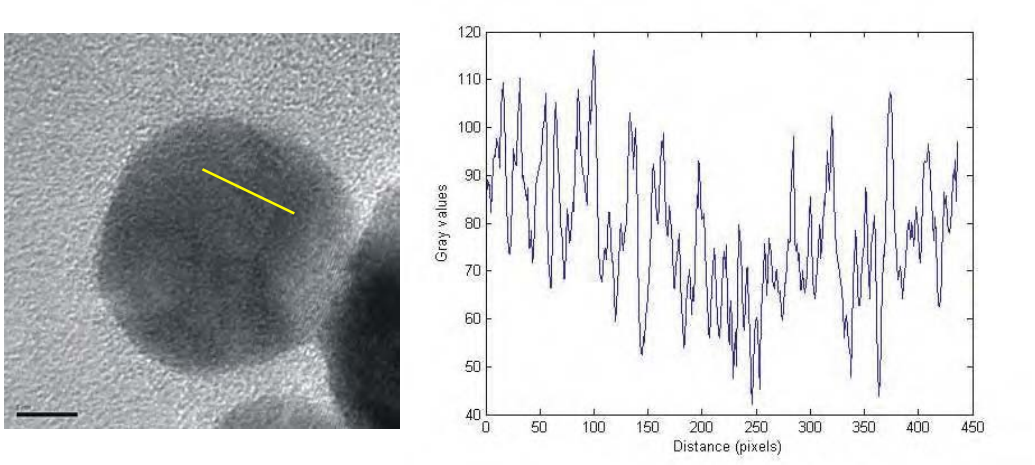

Figure 19. The crystal structure of the AuNP (left). A line plot of the pixels marked in yellow was obtained (right). The distance between the peaks on the graph averaged to 8 pixels which corresponded to a distance of 0.25 nm.

The chemical composition of the nanoparticles was determined, and the energy of the photons emitted from the sample was collected and measured. The spectrum of energies obtained from the citrate-capped AuNP sample is shown in Figure 20. The peaks show the presence of carbon, copper and gold in the sample. The carbon and copper are attributed to the grid on which the particle solution was dried, and the gold is from the nanoparticles. The results from the TEM clearly showed that our solution was indeed colloidal gold nanoparticles with an average diameter of 21 nm.

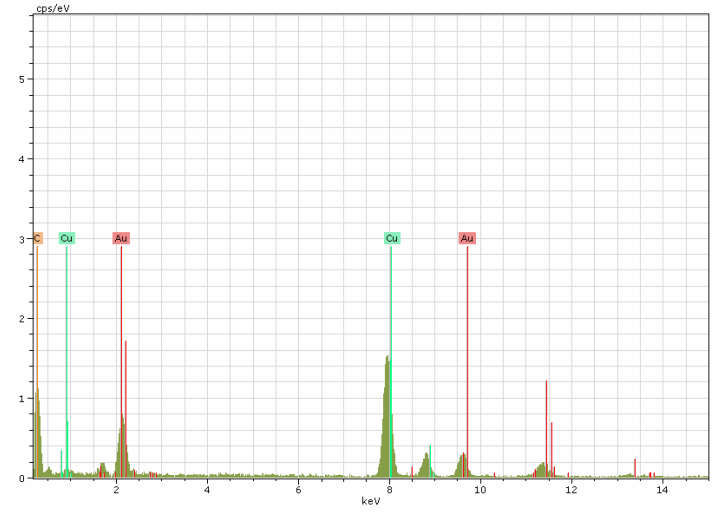

Figure 20. The energies of photons emitted from the AuNP sample

TEM images of the PEGylated AuNP were also obtained at the same magnification as the citrate-capped AuNP (Figure 21). The AuNP were found to be more separated from each other, indicating that the monolayer of PEG chains on the surface of the particles provided enough separation to prevent clumping together. This form of steric stabilization appears to be superior to the electrostatic method which the citrate anions produce.

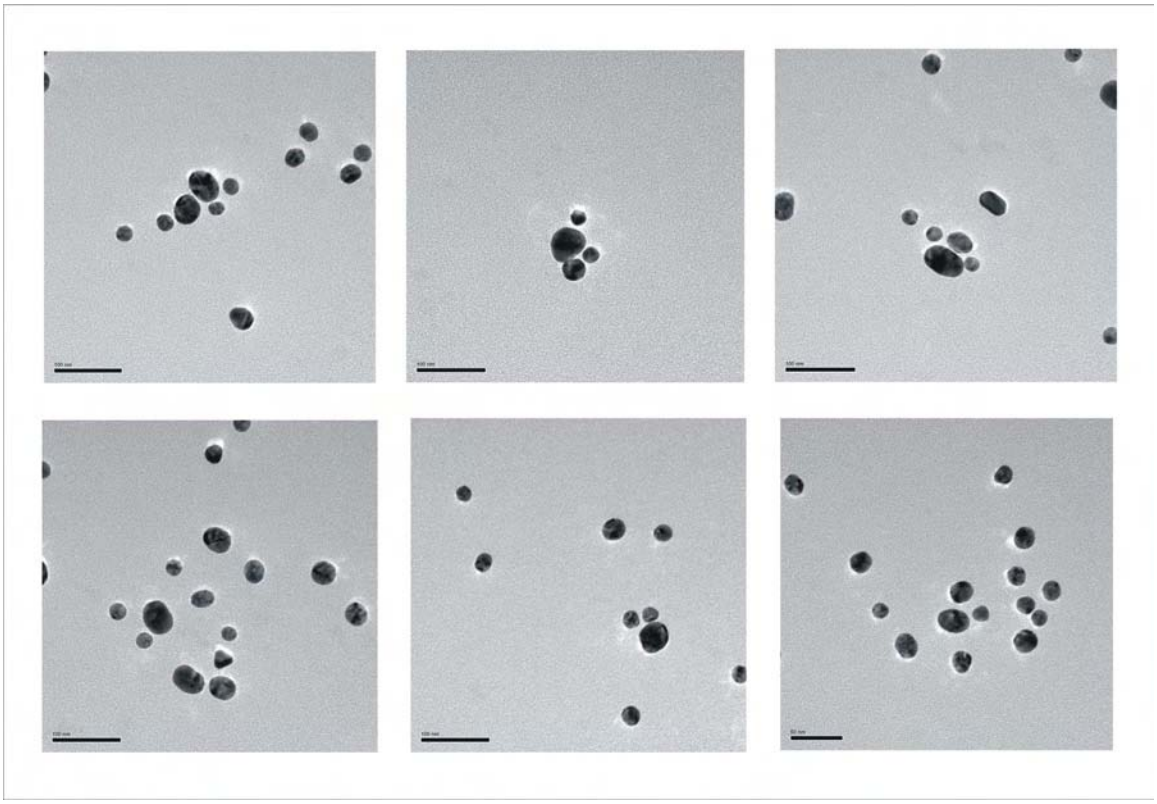

Figure 21. TEM images of PEGylated AuNP

3.2.3 UV-Vis Spectroscopy

Figure 22 shows the UV-Vis spectra of the 14 and 21 nm AuNPs. The spectrum of the 14 nm AuNP (a) shows a peak wavelength at 520 nm, whereas the 21 nm AuNP (b) has a wavelength at 523 nm. The extinction coefficient for 14 and 21 nm AuNP are 1.76×10^8 and 6.31×10^8 $M^{-1}cm^{-1}$. Using the extinction coefficients, the concentrations of the nanoparticles was found to be 7.92 nM and 1.84 nM respectively. The lower

concentration for the larger particle is expected as both colloidal solutions were synthesized using the same amount of starting gold material. The results are summarized in Table 3. Figure 22c shows the two spectra overlaid together after having been normalized for the maximum absorbance. It shows that as the nanoparticle diameter increases, the spectrum shifts to the right and the peak wavelength of the SPR band increases.

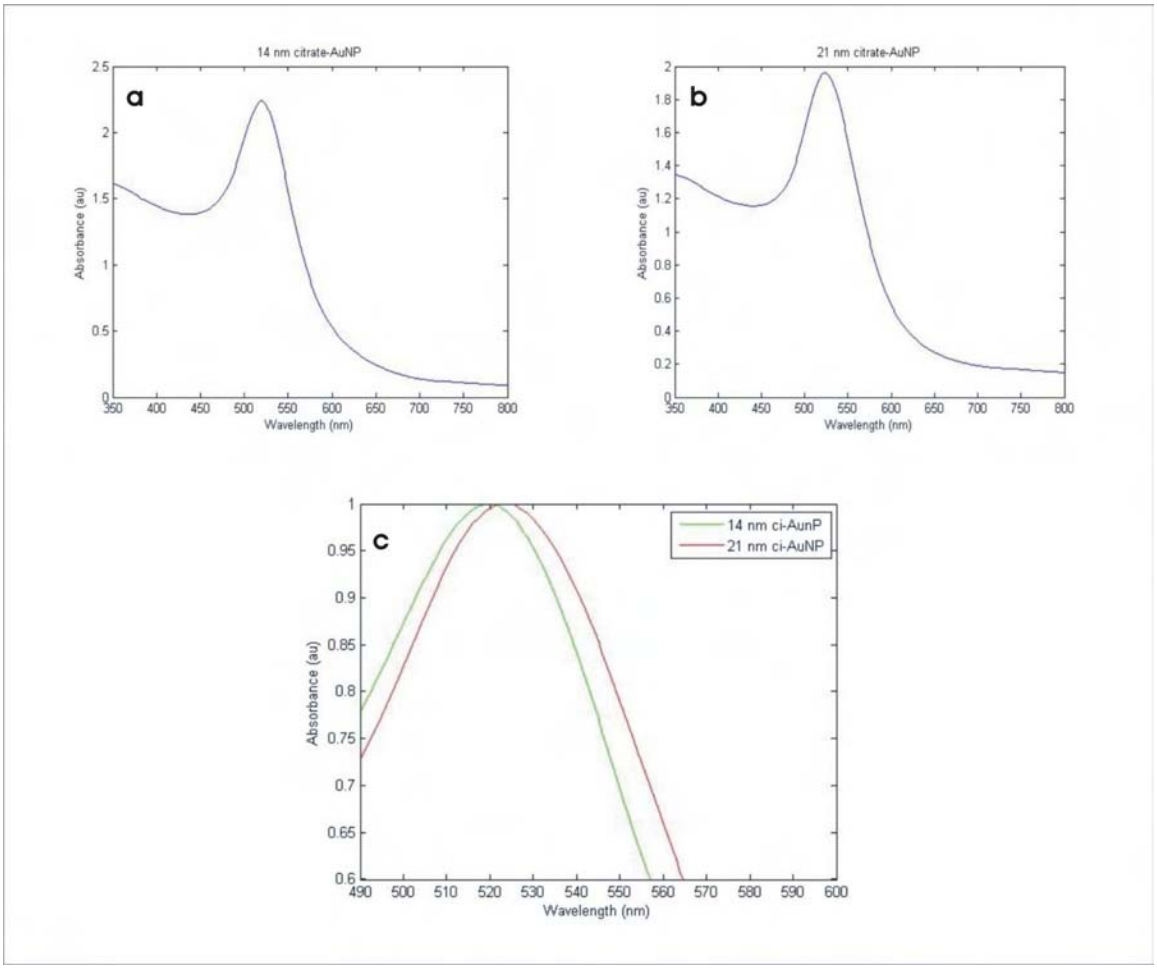

Figure 22. UV/Vis spectra of 14 (a) and 21 (b) nm AuNP, and the two curves overlaid together

Table 3. Summary of results for citrate-capped AuNP

Diameter of AuNP (nm)	Citrate: gold ratio	Concentration (nM)	Peak wavelength of SPR (nm)
14	4 to 1	7.92	520
21	3 to 1	1.84	523

We also investigated the effect of conjugation molecules to the AuNP surface on the position of the SPR band. Figure 23 shows the UV/Vis spectra obtained from adding PEG (a) and PEG and anti-HER2/neu affibodies (b) onto the surface of 21 nm AuNPs. Conjugation of the PEG chains resulted in a 3 nm red shift in the peak wavelength of the SPR band when compared to the citrate-capped AuNP. As the PEG chain is much larger than the citrate anion, the PEGylated AuNP will appear larger than the citrate-capped AuNPs and the peak wavelength of the SPR band will increase. Introducing a mixed monolayer of PEG chains and anti-HER2/neu affibodies onto the AuNP surface, resulted in a further 2 nm red shift in the SPR band from the PEGylated AuNPs. The shift is to be expected as the average molecular weight of the anti-HER2/neu affibody is 14 kDa, while that of the PEG chains is 5 kDa. Adding the affibody onto the surface of the AuNP makes the particle appear larger, resulting in the shift of the SPR band. It is hypothesized that the affibody must extend beyond the layer of PEG chains into the surrounding solution, with its binding site free to interact with the HER2/neu molecule, free from any steric interference from the PEG molecules. This will need to be tested with further experiments in live cell cultures.

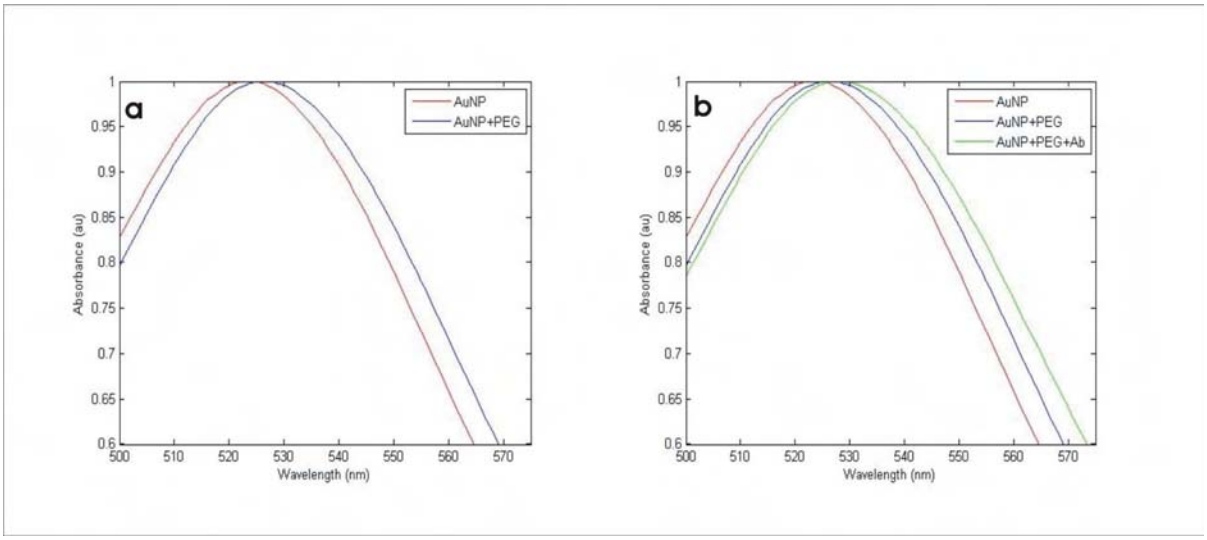

Figure 23. Result of conjugating PEG chains (a) , PEG chains and anti-HER2/neu affibodies (b) onto the surface of 21 nm AuNPs

Table 4. Red shift of conjugated 21 nm AuNP

	Peak wavelength of SPR band (nm)
AuNP (unconjugated, citrate-capped)	523
AuNP + PEG	526
AuNP + PEG + anti-HER2/neu affibody	528

3.2.4 Stability of the citrate-capped AuNPs compared to PEGylated AuNP

The UV/Vis spectrum is also useful in assessing the stability of the nanoparticle solutions in high ionic strength, or salt, media. Although stable in water, the citrate-capped AuNPs were found to aggregate when the 1% PBS solution was added. The color of the resulting solution turned from burgundy to purple-blue, and the spectrum showed a large red-shift and broadening of the plasmon band (Figure 24). By contrast, all of the PEGylated AuNPs were suspended in 1% PBS solution, and as seen in Figures 22 and 23, they were able to maintain the general shape of their absorbance peak. This has strengthened the initial hypothesis that AuNP-PEG conjugates are more stable in salt solutions than their citrate-capped counterparts.

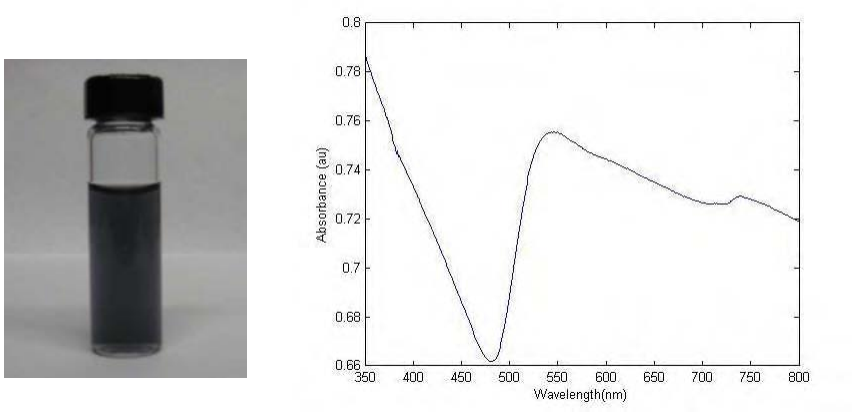

Figure 24. Aggregated citrate-capped AuNPs in 1% PBS solution, and resulting UV-Vis spectrum

4. Discussion and conclusion

4.1 Future Developments

4.1.1 Alternate method for multi-functionalization of AuNPs.

Although the results obtained from the UV/Vis spectroscopy analysis suggested that the HER2/neu affibody conjugation increased the hydrophobic diameter of the AuNP, and extended beyond the influence of the PEG chains, this hypothesis will need to be tested in live cell cultures. An alternative method for the multi-functionalization of the AuNPs could involve a system where the affibody is attached to the distal end of the PEG chain instead of the gold surface. The citrate-capped AuNP would first be quenched with enough PEG to cover the entire surface of the particle. The affibody would then be added, and made to bind to the free end of the PEG chain. In this case, the mPEG-thiol molecule we have used in our conjugation experiments could not be used, as the distal methyl group is unreactive with the cysteine terminal of the affibody. An alternate PEG-derivative could be obtained however, such as thiol-PEG-thiol. This PEG molecule has a reactive thiol group at each end of its chain, and thus could be used to attach to the AuNP surface as well as be conjugated with the anti-HER2/neu affibody (Figure 25).

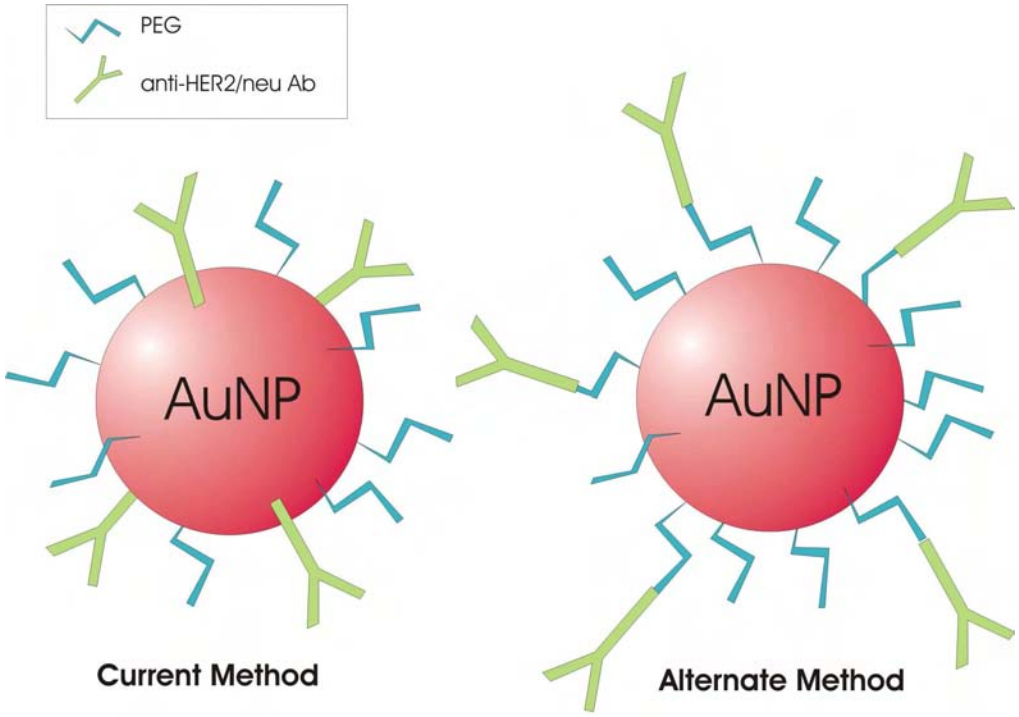

Figure 25. Alternate approach for multi-functionalization of the AuNP

The AuNPs functionalized using the different approaches could then be incubated with cells over-expressing HER2/neu to determine which is more effective in binding with cancer cells. One potential pitfall of the alternate approach would be the tendency of the PEG chains to dimerize, forming sulfide bridges instead of interacting with the cysteine terminal of the affibody. This could possibly be rectified by incubating the PEGylated AuNP into a reducing atmosphere to expose the thiol groups for conjugation before addition of the affibody.

4.1.2 Alternate targets for the AuNPs

We would like to investigate the effects of using other targets, or a combination of targets, for functionalization of the AuNPs. Antibodies against MUC1 or transferrin could be bound to the surface of the AuNPs instead of, or in unison with the HER2/neu affibody. MUC1 has been shown to be more widely expressed in breast cancer cells than

HER2/neu while an anti-transferrin agent would be able to discriminate between rapidly-dividing and idle cells. Such an agent would be able to provide a wealth of valuable information, such as whether an anti-cancer drug has reduced the tumor size or simply stopped it from continued growth. It will also be able to confer whether a drug targeting a specific cell receptor has worked or simply resulted in reduced expression of that receptor on the surface of the cancer cells.

4.1.3 Cell culture

In order to study the uptake pattern of the AuNPs in cancer cells, we will need to culture our own lines of breast cancer cells. Two cell lines have been chosen to represent varying expression of the HER2/neu surface protein: BT-474 and MDA-MB-231. BT-474 shows amplified expression of the protein on its cells surface, whereas MDA-MB-231 shows low to normal expression. In this case, the MDA-MB-231 cells will act as the control to study the non-specific uptake of the AuNPs into cells. The difference in uptake of nanoparticles between the 2 cell lines will help us gauge the effectiveness of our affibody conjugation scheme. The two cells have been widely documented and are readily available by purchase through ATCC (Manassas, VA). BT-474 cells will be grown in RPMI 1640 medium while MDA-MB-231 cells will be grown in Dulbecco's Modified Eagle's Medium (DMEM). For both cells, the base media will be supplemented with 10% fetal bovine serum (FBS), 1% L-glutamine and 1% pen/strep (penicillin/streptomycin). The fetal bovine serum is a common component in many cell cultures and provides many of the necessary nutrients the cells need to grow and proliferate. L-glutamine serves as an extra source of energy and glucose for the cells, while pen/strep helps to treat any bacterial infections that may occur. The concentrations of pen/strep do not hinder the growth of the cancer cells, but can severely inhibit growth

of the much smaller bacteria. Both cells will be cultivated in T-75 flasks and incubated at room temperature (37 ˚C) with 5% CO_2. The cells will be passaged weekly, and the media changed two or three times a week.

Eventually, the cells will be used for imaging. Once there is a sizeable bank for both cell lines, we will begin *in vivo* uptake studies using nude mice. The mice will be injected with a tumoregenic dose of either the BT-474 or MDA-MB-231 cells, administered a solution of the multi-functionalized AuNPs, and subsequently imaged at different time points to determine where the nanoparticles are accumulating.

4.2 Clinical applications for bioconjugated AuNPs

The targeted AuNPs will be especially useful for those tumors that have been pathologically tested to be HER2/neu positive. The nanoparticles can be used to determine if a particular course of therapy has any effect on the cancer cells that over-express the HER2/neu surface protein. The AuNPs can be used to compare the effectiveness of multiple modes of therapy on the cancer cells. We will be able to determine those approaches that result in a reduction in the tumor mass as opposed to simply slowing down the growth rate. The nanoparticles will also be useful in locating potential metastases. Once the primary tumor has been confirmed to be HER2/neu positive, an injection of HER2/neu targeted AuNPs followed by a whole-body CT will uncover whether the cancerous cells have spread to other parts of the body. The nanoparticles will also help better define the spatial extent of the tumor in the body, especially when coupled with the superior spatial resolution obtained by contrast-enhanced DBT. The AuNPs may also provide a valuable tool in the operating room. Images acquired after the surgeon has removed the tumor will be able to quickly determine if indeed all of the cancer cells have been removed.

Conjugation of a wider variety of targeting ligand onto the surface of the AuNPs will result in more information on the tumor being available to the radiologist. Nanoparticles that target cells undergoing rapid cell growth may be able to identify potential tumors that have still not reached a significant size; catching the disease earlier.

4.3 Conclusion

AuNPs were synthesized using a Turkevich approach that involves the reduction of a gold (III) salt by sodium citrate under reflux conditions. The resulting colloidal AuNPs are stabilized in solution by absorbing a monolayer of citrate anions onto their surface. The size of the citrate-capped AuNP was controlled by altering the molar ratio of the gold precursor to the sodium citrate with larger ratios resulting in larger nanoparticles. The AuNPs were then multi-functionalized with a monolayer consisting of an anti-HER2/neu affibody, our targeting ligand, and a poly-ethylene glycol-thiol [37] derivative, our stabilizing agent (Figure 2). HER2/neu belongs to the epidermal growth factor receptor family of surface proteins, and is over-expressed in 25-30% of all breast cancers. The affibody contains a C-terminus cysteine group which allows for direct conjugation with the AuNP surface through the strong thiol-gold interaction. The PEG polymer helps to improve the stability of the AuNP in high ionic strength media, as well as enhance the stealth characteristics of the AuNP *in vivo.* This will increase the longevity of the AuNP in circulation, allowing for sufficient numbers to reach the target tissue without accumulating in the liver and spleen.

The AuNPs were characterized through a combination of small angle x ray scattering (SAXS), transmission electron microscopy (TEM) and UV-Vis spectroscopy. The nanoparticles synthesized using a citrate to gold ratio of 4:1 were confirmed by SAXS to be 14 nm AuNPs, while those produced using a 3:1 ratio were imaged using

TEM and determined to be 21 nm AuNPs. The UV/Vis spectroscopy showed the characteristic absorbance band with a peak wavelength that increased as the diameter of the nanoparticles increased. The functionalization of the AuNPs with the PEG chains caused a 3 nm red shift in the peak wavelength of the SPR band, while the addition of the HER2/neu affibody resulted in a further 2 nm red shift. The PEGylated AuNPs appeared to be more stable in salt solutions and were seen to be spaced further apart when viewed with TEM, as opposed to the citrate-capped particles, which were more clumped together.

There is further work to be conducted including the search for new and alternate targets for the AuNPs. Possible candidates include the MUC1 transmembrane protein which is over-expressed in almost 90% of all breast cancers, and transferrin, which plays a major role in the intake of iron into rapidly growing cancer cells. There are also alternate approaches for the multi-conjugation of the PEG chains and anti-HER2/neu affibodies onto the surface of the AuNP that can be explored, that may reduce the steric interference of the PEG molecule on the efficient binding of the affibody to the target site. The methods can be validated by incubation with breast cancer cell lines that over- and under- express the HER2/neu surface protein.

We believe that the bioconjugated AuNPs can be used as molecular-imaging contrast agents for DBT and DM. The nanoparticles are conjugated to an affinity ligand that will show preferential attachment and internalization by breast cancer cells. The AuNPs will offer an insight into the biological and cellular function of the tumor cells, whether it be the expression level of the HER2/neu surface protein or the proliferation and growth rate of the cells. This functional capability of the bioconjugated AuNPs will

offer a unique insight into the biological state of the tumor cells, providing information that will be useful in both diagnosis and therapy.

References

1. Keidar, Z., O. Israel, and Y. Krausz, *SPECT/CT in tumor imaging: technical aspects and clinical applications.* Seminars in Nuclear Medicine, 2003. **33**(3): p. 205-18.
2. Iagaru, A., X. Chen, and S.S. Gambhir, *Molecular imaging can accelerate anti-angiogenic drug development and testing.* Nature Clinical Practice Oncology, 2007. **4**(10): p. 556-7.
3. Weissleder, R. and U. Mahmood, *Molecular imaging.* Radiology, 2001. **219**(2): p. 316-33.
4. Chen, W., T. Cloughesy, N. Kamdar, et al., *Imaging proliferation in brain tumors with 18F-FLT PET: comparison with 18F-FDG.* Journal of Nuclear Medicine, 2005. **46**(6): p. 945-52.
5. Demura, Y., T. Tsuchida, T. Ishizaki, et al., *18F-FDG accumulation with PET for differentiation between benign and malignant lesions in the thorax.* Journal of Nuclear Medicine, 2003. **44**(4): p. 540-8.
6. Heeren, P.A., P.L. Jager, F. Bongaerts, et al., *Detection of distant metastases in esophageal cancer with (18)F-FDG PET.* Journal of Nuclear Medicine, 2004. **45**(6): p. 980-7.
7. de Geus-Oei, L.F., E.P. Visser, P.F. Krabbe, et al., *Comparison of image-derived and arterial input functions for estimating the rate of glucose metabolism in therapy-monitoring 18F-FDG PET studies.* Journal of Nuclear Medicine, 2006. **47**(6): p. 945-9.
8. Rabinovici, G.D., A.J. Furst, J.P. O'Neil, et al., *11C-PIB PET imaging in Alzheimer disease and frontotemporal lobar degeneration.* Neurology, 2007. **68**(15): p. 1205-12.
9. Buckner, R.L., A.Z. Snyder, B.J. Shannon, et al., *Molecular, structural, and functional characterization of Alzheimer's disease: evidence for a relationship between default activity, amyloid, and memory.* Journal of Neuroscience, 2005. **25**(34): p. 7709-17.
10. Kemppainen, N.M., S. Aalto, I.A. Wilson, et al., *PET amyloid ligand [11C]PIB uptake is increased in mild cognitive impairment.* Neurology, 2007. **68**(19): p. 1603-6.
11. Caravan, P., J.M. Greenwood, J.T. Welch, et al., *Gadolinium-binding helix-turn-helix peptides: DNA-dependent MRI contrast agents.* Chemical Communications, 2003(20): p. 2574-5.
12. *Molecular Imaging: Companies set out to sharpen the in vivo perspective with new machines and novel contrast angets.* Chemical and Engineering News, 2005. **83**(30): p. 25-34.
13. Gommersall, L., I.S. Shergill, H.U. Ahmed, et al., *Nanotechnology and its relevance to the urologist.[see comment]*. European Urology, 2007. **52**(2): p. 368-75.
14. Jain, T.K., M.A. Morales, S.K. Sahoo, et al., *Iron oxide nanoparticles for sustained delivery of anticancer agents.* Molecular Pharmaceutics, 2005. **2**(3): p. 194-205.

15. Badea, C.T., E. Bucholz, L.W. Hedlund, et al., *Imaging methods for morphological and functional phenotyping of the rodent heart.* Toxicologic Pathology, 2006. **34**(1): p. 111-7.
16. Krausz, Y., Z. Keidar, I. Kogan, et al., *SPECT/CT hybrid imaging with 111In-pentetreotide in assessment of neuroendocrine tumours.* Clinical Endocrinology, 2003. **59**(5): p. 565-73.
17. Dvorak, H.F., T.M. Sioussat, L.F. Brown, et al., *Distribution of vascular permeability factor (vascular endothelial growth factor) in tumors: concentration in tumor blood vessels.* Journal of Experimental Medicine, 1991. **174**(5): p. 1275-8.
18. Rode, U. and R. Muller, *Transformation of the ionic X-ray contrast agent diatrizoate and related triiodinated benzoates by Trametes versicolor.* Appl Environ Microbiol, 1998. **64**(8): p. 3114-7.
19. Dvorak, H.F., J.A. Nagy, J.T. Dvorak, et al., *Identification and characterization of the blood vessels of solid tumors that are leaky to circulating macromolecules.* American Journal of Pathology, 1988. **133**(1): p. 95-109.
20. Nagy, J.A., L.F. Brown, D.R. Senger, et al., *Pathogenesis of tumor stroma generation: a critical role for leaky blood vessels and fibrin deposition.* Biochimica et Biophysica Acta, 1989. **948**(3): p. 305-26.
21. Hainfeld, J.F., D.N. Slatkin, T.M. Focella, et al., *Gold nanoparticles: a new X-ray contrast agent.* Br J Radiol, 2006. **79**(939): p. 248-53.
22. Chen, S.C., A.K. Carton, M. Albert, et al., *Initial clinical experience with contrast-enhanced digital breast tomosynthesis.* Academic Radiology, 2007. **14**(2): p. 229-38.
23. Lindfors, K.K., J.M. Boone, T.R. Nelson, et al., *Dedicated breast CT: initial clinical experience.* Radiology, 2008. **246**(3): p. 725-33.
24. Yang, K., A.L. Kwan, D.F. Miller, et al., *A geometric calibration method for cone beam CT systems.* Medical Physics, 2006. **33**(6): p. 1695-706.
25. Jong, R.A., M.J. Yaffe, M. Skarpathiotakis, et al., *Contrast-enhanced Digital Mammography: Initial Clinical Experience.* Radiology, 2003. **228**(3): p. 842-850.
26. Tkachenko, A., H. Xie, S. Franzen, et al., *Assembly and characterization of biomolecule-gold nanoparticle conjugates and their use in intracellular imaging.* Methods in Molecular Biology, 2005. **303**: p. 85-99.
27. Tkachenko, A.G., H. Xie, D. Coleman, et al., *Multifunctional gold nanoparticle-peptide complexes for nuclear targeting.* Journal of the American Chemical Society, 2003. **125**(16): p. 4700-1.
28. Moses, S., S.H. Brewer, L.B. Lowe, et al., *Characterization of single- and double-stranded DNA on gold surfaces.* Langmuir, 2004. **20**(25): p. 11134-40.
29. Niidome, T., M. Yamagata, Y. Okamoto, et al., *PEG-modified gold nanorods with a stealth character for in vivo applications.* Journal of Controlled Release, 2006. **114**(3): p. 343-7.
30. Niidome, Y., K. Honda, K. Higashimoto, et al., *Surface modification of gold nanorods with synthetic cationic lipids.* Chemical Communications, 2007(36): p. 3777-9.
31. Hainfeld, J.F., F.A. Dilmanian, D.N. Slatkin, et al., *Radiotherapy enhancement with gold nanoparticles.* J Pharm Pharmacol, 2008. **60**(8): p. 977-85.

32. Kimling, J., M. Maier, B. Okenve, et al., *Turkevich method for gold nanoparticles revisited.* Journal of Physical Chemistry, 2006. **110**: p. 15700-15707.
33. Liu, Y., M.K. Shipton, J. Ryan, et al., *Synthesis, stability, and cellular internalization of gold nanoparticles containing mixed peptide-poly(ethylene glycol) monolayers.* Analytical Chemistry, 2007. **79**(6): p. 2221-9.
34. Murray, R.W., *Nanoelectrochemistry: metal nanoparticles, nanoelectrodes, and nanopores.* Chem Rev, 2008. **108**(7): p. 2688-720.
35. Chithrani, B.D. and W.C. Chan, *Elucidating the mechanism of cellular uptake and removal of protein-coated gold nanoparticles of different sizes and shapes.* Nano Letters, 2007. **7**(6): p. 1542-50.
36. Grabar, K., R. Greeman, M. Hommer, et al., *Preperation and characterization of Au Colloid monolayers.* Analytical Chemistry, 1995. **67**: p. 735-743.
37. Pegram, M.D., A. Lipton, D.F. Hayes, et al., *Phase II study of receptor-enhanced chemosensitivity using recombinant humanized anti-p185HER2/neu monoclonal antibody plus cisplatin in patients with HER2/neu-overexpressing metastatic breast cancer refractory to chemotherapy treatment.* Journal of Clinical Oncology, 1998. **16**(8): p. 2659-71.
38. Brewer, S.H., W. Glomm, M. Johnson, et al., *Probing BSA binding to citrate-coated gold nanoparticles and surfaces.* Langmuir, 2005. **21**: p. 9303-9307.
39. Zheng, M., F. Davidson, and X. Huang, *Ethylene glycol monolayer protected nanoparticles for eliminating nonspecific binding with biological molecules.* Journal of the American Chemical Society, 2003. **125**(26): p. 7790-1.
40. Zheng, M., Z. Li, and X. Huang, *Ethylene glycol monolayer protected nanoparticles: synthesis, characterization, and interactions with biological molecules.* Langmuir, 2004. **20**(10): p. 4226-35.
41. Tonik, S.E., J.E. Shindelman, and H.H. Sussman, *Transferrin receptor is inversely correlated with estrogen receptor in breast cancer.* Breast Cancer Research & Treatment, 1986. **7**(2): p. 71-6.
42. Nikinmaa, B., C.A. Enns, S.E. Tonik, et al., *Monoclonal antibodies to a purified human transferrin receptor.* Scandinavian Journal of Immunology, 1984. **20**(5): p. 441-7.
43. Moore, A., Z. Medarova, A. Potthast, et al., *In vivo targeting of underglycosylated MUC-1 tumor antigen using a multimodal imaging probe.* Cancer Research, 2004. **64**(5): p. 1821-7.
44. Baselga, J., A.D. Seidman, P.P. Rosen, et al., *HER2 overexpression and paclitaxel sensitivity in breast cancer: therapeutic implications.* Oncology (Williston Park), 1997. **11**(3 Suppl 2): p. 43-8.
45. Baselga, J., D. Tripathy, J. Mendelsohn, et al., *Phase II study of weekly intravenous recombinant humanized anti-p185HER2 monoclonal antibody in patients with HER2/neu-overexpressing metastatic breast cancer.[see comment]*. Journal of Clinical Oncology, 1996. **14**(3): p. 737-44.
46. Molina, M.A., J. Codony-Servat, J. Albanell, et al., *Trastuzumab (herceptin), a humanized anti-Her2 receptor monoclonal antibody, inhibits basal and activated Her2 ectodomain cleavage in breast cancer cells.* Cancer Research, 2001. **61**(12): p. 4744-9.

47. *The transmission electron microscope*. [cited Aug. 3 2008]; Available from: http://nobelprize.org/educational_games/physics/microscopes/tem/index.html.
48. Reimer, L., *Transmission electron microscopy: Physics of image formation and microanalysis*. 4th ed. 1997, Berlin Springer-Velag. 584.
49. Diaz, A., T. Weitkamp, H. Jeyemeulen, et al., *SAXS studies of colloid solutions.* 2003.
50. Nagao, O., G. Haraga, T. Sugawara, et al., *Small-angle x-ray scattering method to determine the size distribution of gold nanoparticles chemisorbed by thiol ligands.* Japanese Journal of Applied Physics, 2004. **43**: p. 7742-7746.
51. Haiss, W., N.T. Thanh, J. Aveyard, et al., *Determination of size and concentration of gold nanoparticles from UV-vis spectra.* Analytical Chemistry, 2007. **79**(11): p. 4215-21.
52. Kelly, K., E. Coronado, L. Xhao, et al., *The optical properties of metal nanoparticles: The influence of size, shape, and dielectric environment.* Journal of Physical Chemistry, 2003. **107**: p. 668-677.
53. Maeland, A. and T.B. Flanagan, Journal of Physical Chemistry, 1968: p. 1419.